

## Article

# Study on the Coupled Heat Transfer of Conduction, Convection, and Radiation in Foam Concrete Based on a Microstructure Numerical Model

Tao Huang <sup>1,2,\*</sup>, Mengge Wang <sup>1,2</sup>, Shuang Feng <sup>1,2</sup>, Zhongqi Peng <sup>1,2</sup>, Xiaoyu Huang <sup>3</sup> and Yaohua Song <sup>4</sup>

<sup>1</sup> School of Engineering, Architecture and the Environment, Hubei University of Technology, Wuhan 430086, China; 102100762@hbut.edu.cn (M.W.); 102110888@hbut.edu.cn (S.F.); 102110878@hbut.edu.cn (Z.P.)

<sup>2</sup> Key Laboratory of Intelligent Health Perception and Ecological Restoration of Rivers and Lakes, Ministry of Education, Hubei University of Technology, Wuhan 430086, China

<sup>3</sup> School of Civil, Environmental Engineering and Geography Science, Ningbo University, Ningbo 315211, China; huangxiaoyu202203@163.com

<sup>4</sup> Faculty of Science, The University of New South Wales, Sydney, NSW 2052, Australia; z5494314@ad.unsw.edu.au

\* Correspondence: httcmwh@hbut.edu.cn

**Abstract:** Foam concrete is a typical cement-based porous material; its special microstructure endows it with excellent properties, such as light weight, energy efficiency, thermal insulation, and fire resistance. Therefore, it is widely used as a thermal insulation material for buildings. The heat transfer modes of foam concrete include conduction, convection, and radiation. However, previous studies considered conduction to be the dominant mode, often neglecting the effects of convection and radiation. In this study, a stochastic numerical model of the foam concrete microstructure is established based on the statistical parameters of the pore structure. With this model, the heat transfer mechanism of foam concrete is analyzed at the mesoscopic level, and the equivalent thermal conductivity is calculated. By comparing four different working conditions, the influence of conduction, convection, and radiation on the heat transfer of foam concrete is analyzed, and the specific contribution rates of conduction, convection, and radiation are calculated. The results show that the convection effect is weak due to the pore size being smaller than 1 mm; so, the influence of convection can be neglected in the heat transfer analysis of foam concrete. The contribution of radiation increases with the decrease in foam concrete density and the increase in temperature difference. When the temperature difference is 40 °C and the density is 300 kg/m<sup>3</sup>, the contribution of radiation exceeds 20%. Therefore, for low-density and high-temperature difference situations, the influence of radiation cannot be ignored. The heat transfer in foam concrete is mainly through conduction, but with the decrease in density and the increase in temperature difference, the contribution of conduction shows a downward trend. Nevertheless, the contribution of conduction is still much larger than that of radiation and convection.

**Keywords:** foam concrete; microstructure; coupled heat transfer; equivalent thermal conductivity



**Citation:** Huang, T.; Wang, M.; Feng, S.; Peng, Z.; Huang, X.; Song, Y. Study on the Coupled Heat Transfer of Conduction, Convection, and Radiation in Foam Concrete Based on a Microstructure Numerical Model. *Buildings* **2024**, *14*, 1287. <https://doi.org/10.3390/buildings14051287>

Academic Editor: Sufen Dong

Received: 26 March 2024

Revised: 23 April 2024

Accepted: 29 April 2024

Published: 2 May 2024



**Copyright:** © 2024 by the authors. Licensee MDPI, Basel, Switzerland. This article is an open access article distributed under the terms and conditions of the Creative Commons Attribution (CC BY) license (<https://creativecommons.org/licenses/by/4.0/>).

## 1. Introduction

With the rapid development of the economy and society, the issue of energy consumption is becoming increasingly severe. In 2021, the energy consumption of the construction and operation of buildings in China accounted for about 31% of the total energy consumption [1–4]. Currently, using insulation materials in buildings is a widely adopted solution [5,6]. Expanded polystyrene (EPS) and polyurethanes (PUs) are common insulation materials for achieving energy savings in buildings due to their excellent thermal insulation properties, light weight, and unique waterproof performance [7,8]. However, despite their many advantages, these polymer foams have poor resistance to high temperatures and poor fire safety. Fires caused by organic insulation materials have resulted

in huge economic losses and numerous casualties [9–11]. In contrast, incombustible inorganic insulation materials exhibit commendable fire resistance and have broad application prospects in the field of thermal insulation. Among inorganic insulation materials, foam concrete is a thermal insulation material that contains a large number of honeycomb-like pores, formed by the mixing of pre-fabricated foam with cement slurry [4]. Due to its large number of closed honeycomb structures, foam concrete has low self-weight, excellent thermal insulation, and excellent fire resistance compared to traditional concrete, making it a promising insulation material [12,13]. The macroscopic properties of cementitious materials are closely related to their microstructures. V. Ducman et al. detected changes in porosity in systematic foams by X-CT tomography to assess the effect on their macroscopic properties [14]. Behnam Mobaraki et al. proposed an algorithm for an observability analysis of two-dimensional cellular structures, which provides a new approach for applications in characterizing concrete structures [15]. Studies on the preparation of foam concrete have shown that its density grade ranges from 300 to  $1700 \text{ kg/m}^3$  and that its porosity is between 0.1 and 0.9 [16–20]. The effect of fly ash and silica fume admixture on compressive strength and thermal conductivity of foam concrete was investigated by H. Süleyman Gökçe et al. [21]. Ehsan Hosseinzadehfard and Behnam Mobaraki presented the effect of partial substitution of natural volcanic ash for micro silica clay on the strength and durability of concrete, and their study provides a practical method for designing concrete applications at a significantly reduced cost [22]. Foam concrete has a broad application prospect. Currently, it has been widely used in roof insulation, road base layers, building partitions, and foundation compensation, among other areas. Amritha Raj et al. produced foam concrete insulation boards using cement, straw, and fly ash as raw materials, and numerically simulated the thermal insulation performance of insulated external walls using COMSOL software [23]. Zening Li et al. considered the uncertainty of sunlight and used building thermodynamics to analyze the comfortable temperature range of buildings [24].

The prediction of the effective thermal conductivity of porous materials is a traditional problem, and various models have been developed to determine the thermal conductivity of porous materials in the design of building thermal insulation performance. These models can be divided into three categories: (1) analytical models obtained by solving two-dimensional or three-dimensional Laplace heat conduction equations, (2) empirical correlation models, and (3) numerical simulation models [25].

Classic analytical models have general applicability, but they simplify the structure and mathematical assumptions to some extent. For example, one assumption of the Maxwell–Eucken model is that the dispersed phase exists independently within the continuous phase, which means there is no interaction between the dispersed phase and the components [26]. The EMPT model assumes that all the components are completely randomly distributed and that any component can form a continuous thermal conduction path, depending on its volume fraction [27–29]. These analytical models are based on idealized structures; consequently, their wide applicability to real engineering porous media is limited.

Empirical correlations are based on the curve fitting of experimental data for several types of porous materials using empirical constants; therefore, their accuracy is closely related to the experimenter's technical methods or the precision of the testing equipment. The analyses of some of the theoretical and empirical models for predicting thermal conductivity that have been proposed in the literature suggest that idealized analytical models may not be suitable for low-density porous materials and could lead to incorrect predictions; the energy transfer process in porous materials is more complex, and the assumption that conduction is the only mode of energy transfer is not applicable to porous materials under all conditions.

In recent years, the finite element analysis method based on equation space discretization has been widely used by researchers in solving mathematical models [30–32]. A vast amount of the literature on the thermal analysis of porous materials indicates that numerical analysis is a feasible approach for the prediction of the thermal conductivity of porous materials [33–36]. R. Coquard et al. calculated the effective thermal conductivity of

heterogeneous porous materials using the numerical finite volume method [37]. Sharma employed the finite element simulation method to study the steady-state heat transfer of composite materials and predicted the effective thermal conductivity of polyhedral and spherical inclusions [30]. Miled et al. derived various analytical forms of effective thermal conductivity based on a homogenization scheme and obtained numerical results using three-dimensional finite element method (FEM) simulations on ideal foam concrete [38].

As the main mechanism of heat transfer is thermal conduction, most studies currently focus on the description of thermophysical properties generated by conductive transmission [39,40]. Some of the studies have found that the underestimation of the equivalent thermal conductivity may be due to the neglect of radiation, and related studies indicate that the contribution of radiation accounts for 6–30% of the overall equivalent thermal conductivity [37,39,41]. The literature is extensive, with very detailed numerical studies of convective and radiative coupled heat transfer in polymer foams. Sepehri et al. successfully simulated the flow and heat transfer in open-cell metal foams using a pore-scale analysis method and found that at high Reynolds numbers, the convective heat transfer mechanism became more significant; they conclude that neglecting this mechanism would lead to errors in the results [42]. Fan et al. established numerical models for open-cell foams of different shapes based on computed tomography and Cinema 4D, solving the coupled heat transfer energy equation. They studied the influence of pore shape on conductive–radiative heat transfer behavior and provided a comprehensive approach to the investigation of the conductive radiative coupled heat transfer in alumina foam [43]. Li et al. solved the natural convection heat transfer problem in a closed cavity using the pure finite volume method, the pure lattice Boltzmann method, and different lattice Boltzmann coupling methods, respectively. By comparing the conclusions drawn from different methods, they found that the coupling method was a reliable approach for solving natural convection problems [44]. Wei et al. (2023) proposed a unified lattice Boltzmann model to solve the radiative–conductive coupled heat transfer problem, and the applicability and accuracy of the numerical model were verified through numerical examples [45]. In most cases, convective and radiative heat transfer is neglected because convection within pores is considered negligible when the pore size is smaller than 4 mm, and radiation usually accounts for a small proportion of the heat transfer of foam concrete [46–49]. Therefore, there has been no numerical simulation of convective and radiative coupled heat transfer in foam concrete. Although existing numerical models can consider the randomness and complexity of the microstructure, they only address heat transfer problems under pure conduction. There is limited involvement in the study of convective heat transfer and radiative coupled heat transfer within pores, and no studies have been conducted on convective and radiative heat transfer in foam concrete using real microstructures [50].

In summary, the current research on the heat transfer of foam concrete mainly focuses on conduction, and less consideration is given to the effects of convection and radiation. However, studies on other porous materials have shown that under certain conditions, the contributions of convection and radiation to heat transfer cannot be ignored. To study the coupled heat transfer mechanism of foam concrete, the organizational structure of this study is as follows: Section 2 elaborates in detail on the mechanism of heat transfer in foam concrete, listing the control equations for conduction, convection, and radiation heat transfer. Section 3 describes the method for establishing a microstructural numerical model and designs multiple working condition simulation schemes for different heat transfer modes. Section 4 presents the research results, including model validation, the equivalent thermal conductivity is calculated, the heat transfer rules of foam concrete under different heat transfer modes are analyzed, and the contribution rates of conduction, convection, and radiation to heat transfer are calculated. Finally, the main conclusions of this study are outlined in Section 5.

## 2. Heat Transfer Mechanism

Foam concrete can be regarded as a two-phase material composed of a hardened cementitious matrix and air; macroscopically, the inhomogeneous material can be considered as a homogeneous medium [50]. Therefore, heat transfer in foam concrete includes thermal conduction through the solid matrix, thermal conduction and convection in the gas-filled pores, and thermal radiation between different parts of the material.

### 2.1. Thermal Conduction

The primary mode of heat transfer in foam concrete is thermal conduction, which relies on the thermal motion of molecules to transfer heat energy without requiring relative displacement between different parts of the object. Thermal conduction in foam concrete includes both conduction between solid phases and conduction between gas phases. Assuming that the material is isotropic, the governing equation for steady-state thermal conduction is as follows [51]:

$$\nabla \cdot \mathbf{q} = Q \quad (1)$$

where  $\mathbf{q}$  is the heat flux ( $\text{W}/\text{m}^2$ ),  $Q$  is the internal heat source strength (J), and  $\nabla$  is the Hamiltonian operator.

According to Fourier's law:

$$\mathbf{q} = -k\nabla T \quad (2)$$

where  $k$  is the thermal conductivity of the material ( $\text{W}/\text{mK}$ ), and  $T$  is the temperature field function (K). Substituting (2) into (1) yields

$$-k\nabla^2 T = Q \quad (3)$$

In the case where only thermal conduction is considered, both the solid-phase matrix and the air in the pores of foam concrete satisfy Equation (3). At the interface between the solid and gas phases (i.e., at the surface of the pores), the conditions of temperature continuity and heat flux density continuity must be met, as follows

$$\begin{cases} T_s = T_g \\ k_s \frac{\partial T_s}{\partial \mathbf{n}} = k_g \frac{\partial T_g}{\partial \mathbf{n}} \end{cases} \quad (4)$$

where  $T_s$  and  $T_g$  represent the temperatures of the matrix and air (K), respectively,  $k_s$  and  $k_g$  represent the thermal conductivities of the matrix and air ( $\text{W}/\text{mK}$ ), respectively, and  $\mathbf{n}$  represents the outward normal to the boundary.

### 2.2. Thermal Convection

The pores of foam concrete are filled with air, and the flow and heat transfer of air follow the three conservation laws of mass, momentum, and energy conservation. Assuming that the air is an ideal gas and neglecting viscous heating and the work carried out by gas pressure, the Navier Stokes equations for steady-state conditions can be expressed in the following form [51].

Continuity equation

$$\nabla \cdot (\rho \mathbf{u}) = 0 \quad (5)$$

Momentum equation

$$\rho \mathbf{u} \cdot \nabla \mathbf{u} = -\nabla p + \nabla \cdot \mu (\nabla \mathbf{u} + (\nabla \mathbf{u})^T) - \frac{2}{3} \nabla (\mu (\nabla \cdot \mathbf{u})) + \rho \mathbf{g} + \mathbf{f} \quad (6)$$

Energy equation

$$\rho c \mathbf{u} \cdot \nabla T - k \nabla^2 T = Q \quad (7)$$

In the equations above,  $\mathbf{u}$  is the air velocity vector ( $\text{m}/\text{s}$ ),  $c$  is the specific heat capacity of air at constant pressure ( $\text{J}/\text{kgK}$ ),  $\rho$  is the air density ( $\text{kg}/\text{m}^3$ ),  $\mathbf{g}$  is the acceleration due to

gravity ( $\text{kg}$ ),  $p$  is the air pressure ( $\text{pa}$ ),  $\mu$  is the dynamic viscosity of air ( $\text{pa/s}$ ), and  $\rho\mathbf{g}$  and  $\mathbf{f}$  ( $\text{N}$ ) are the gravitational and other external body forces, respectively. When the velocity  $\mathbf{u}$  in Equation (7) is set to zero, Equation (7) reduces to Equation (3); thus, Equation (7) can uniformly describe the heat transfer characteristics of both the solid and gas phases.

The coupling of conduction and convection involves not only the coupling of the flow field and temperature field but also the heat transfer coupling between the fluid and solid.

### 2.3. Thermal Radiation

Radiative heat transfer refers to the transfer of energy by objects through electromagnetic waves. In foam concrete, there are many pores and heat exchange can occur between pore surfaces through radiation. Assuming that the pore surfaces are opaque, diffuse gray surfaces and that the air in the pores is absolutely transparent and does not participate in radiative heat exchange, the heat flux density  $q_\gamma(x)$  caused by radiation at the pore surfaces satisfies the following integral equation [51]:

$$\frac{q_\gamma(x)}{\gamma(x)} = eT^4(x) + \int_\Gamma \frac{1-\gamma(y)}{\gamma(y)} q_\gamma(y) \omega^*(x,y) d\Gamma(y) - \int_\Gamma eT^4(y) \omega^*(x,y) d\Gamma(y), \quad x, y \in \Gamma \quad (8)$$

In the equation,  $q_\gamma(x)$  the heat flux density ( $\text{W/m}^2$ ),  $\gamma(x)$  represents the emissivity of the pore surface,  $e$  is the blackbody radiation constant,  $\omega^*(x,y)$  is the radiation view factor, and  $\Gamma$  represents the area of the pore surface.

The coupled equation of thermal radiation and thermal conduction at the pore surface can be expressed as follows:

$$-k_s \frac{\partial T_s}{\partial \mathbf{n}} = q_\gamma(x) \quad (9)$$

## 3. Numerical Model

To predict the effective thermal conductivity of foam concrete, most analytical models consider the thermal conductivities and volume fractions of the matrix and pores as important parameters, while neglecting the randomness of the pore size and distribution. However, the impact of randomness on the thermal performance of foam concrete is a subject that warrants further investigation.

In this study, based on the statistical laws of pore size in foam concrete, a random numerical model of the foam concrete microstructure is constructed using a method that randomly places a certain number of circular pores of a certain size within a given area. This model is then imported into the finite element software COMSOL (6.0 Version, COMSOL Inc., Stockholm, Sweden). By considering the coupling of different heat transfer modes, assigning material parameters, and applying boundary conditions, a steady-state heat transfer analysis is conducted on the model, and the model's effective thermal conductivity is calculated.

### 3.1. Pore Microstructure Modeling

To establish a numerical model of the foam concrete microstructure, the following assumptions are made:

1. The pores in foam concrete are approximately circular in shape, and the pore size approximately follows a log-normal distribution, whose probability density function can be represented as follows [52]

$$f_d(d; \mu, \sigma) = \frac{1}{d\sigma\sqrt{2\pi}} e^{-\frac{(\ln d - \mu)^2}{2\sigma^2}}, \quad d > 0 \quad (10)$$

2. The distribution of pores is random and uniform, meaning that any point in the plane has an equal probability of becoming the center of a circle. Therefore, based

on the uniform distribution function, the coordinates of the circle centers can be randomly generated.

Under the aforementioned assumptions, the main modeling steps are as follows:

3. Generate a standard library of pore sizes. Based on the given statistical parameters of pore size  $\mu$  and  $\sigma$ , set the minimum pore size to  $d_{min} = e^{\mu-3\sigma}$  and the maximum pore size to  $d_{max} = e^{\mu+3\sigma}$  to ensure that 99.7% of the pore sizes fall within this interval. Within this interval, randomly generate  $m$  pore sizes using the log-normal distribution, and store the generated pore sizes in descending order in an array  $D$  to form the standard library of pore sizes.
4. Placement of pores. Sequentially take a pore size value from array  $D$  and, based on the uniform distribution function, randomly generate the center coordinates of the pore within the placement area. To simulate the phenomenon of pores overlapping and merging with each other in foam concrete, define the overlap ratio  $\delta$ : the ratio of the overlapping area of two circles to the smaller of the two circle areas, which represents the degree of merging between pores. When the overlap ratio between a newly placed pore and an already successfully placed pore is greater than the set value  $\delta$ , the placement of that pore needs to be redone, i.e., the center coordinates of the pore need to be regenerated, until the overlap ratio between that pore and other pores is less than or equal to the set value  $\delta$ .
5. Porosity calculation. As there is an overlap between pores, and the overlapping part is random, the actual porosity of the model cannot be obtained through theoretical calculations. In this study, the 'lattice method' is used to calculate the actual porosity of the model more accurately. The placement area is divided into  $n$  equal-length, equal-width rectangles. If the center of a rectangle is inside a circular pore (i.e., the distance between the center of the rectangle and the center of the circle is less than the radius of the circle), then the area of the rectangle is considered to be part of a pore; otherwise, it is considered to be part of the matrix. The number of rectangles considered to be part of the pores is counted and then divided by the total number of rectangles  $n$  to obtain the actual porosity of the model  $\varepsilon'$ . Clearly, the more rectangles the area is divided into, the more accurate the porosity calculation. If the difference between the actual porosity  $\varepsilon'$  and the desired porosity  $\varepsilon$  is less than a given error limit, the model is considered satisfactory, and the modeling process is complete. Otherwise, adjust the number of pores  $m$ , and start over from step 1, until the porosity meets the requirements.

Implement random generation in MATLAB according to the aforementioned generation steps, with the process flowchart shown in Figure 1.

The numerical models of the microstructure of foam concrete with densities of  $800 \text{ kg/m}^3$  and  $500 \text{ kg/m}^3$  (the modeling pore parameters are derived from the experiments of She [33]), which were generated according to the above method, are shown in Figure 2. In the figure, the blue area represents the solid phase and the white area represents the gas phase. The randomly generated microstructural numerical models are relatively close to the actual pore structure in terms of morphology.

### 3.2. Boundary Conditions and Material Parameters

The generated numerical model of the foam concrete microstructure was imported into the finite element software COMSOL (6.0 Version, COMSOL Inc., Stockholm, Sweden) to simulate the steady-state heat transfer in a porous medium without internal heat sources, as shown in Figure 3. Different temperature loads ( $T_{cold}$ ,  $T_{hot}$ ) were applied to the top and bottom of the specimen to create a temperature gradient, and heat flowed from the bottom to the top of the specimen. The left and right sides of the specimen were in an adiabatic state. The pores contained air, and the surfaces of the pores served as both walls for the air flow and as surfaces for the thermal radiation.

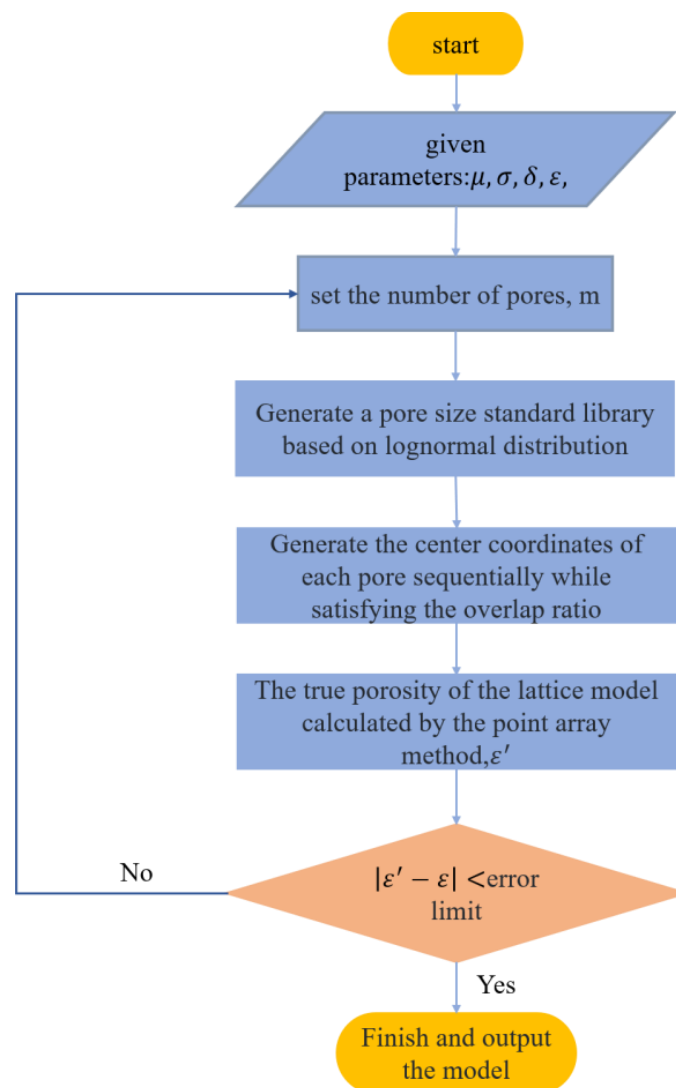


Figure 1. Modeling process diagram.

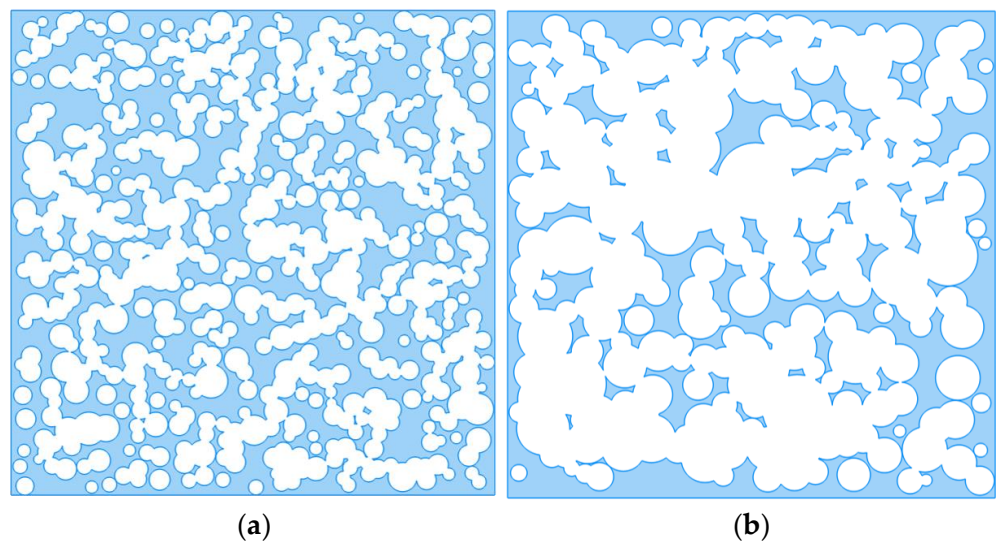
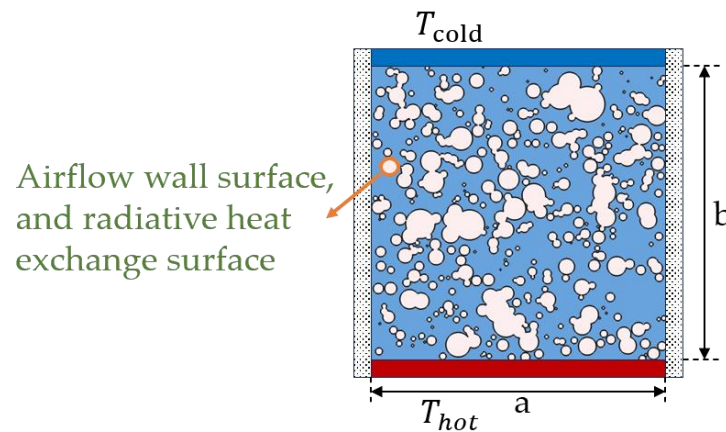


Figure 2. Numerical model of foam concrete: (a) 800 kg/m<sup>3</sup>,  $\epsilon = 59\%$ ; (b) 500 kg/m<sup>3</sup>,  $\epsilon = 75.45\%$ .



**Figure 3.** Boundary condition setting.

Using COMSOL (6.0 Version, COMSOL Inc., Stockholm, Sweden), simulations were conducted for four different conditions (the details of the four conditions are provided in Table 1). Steady-state heat transfer analysis was performed for these four conditions, and the effective thermal conductivity of the specimen under each condition was calculated using the following formula:

$$k_i = \frac{bQ_{tot}}{a(T_{hot} - T_{cold})} \quad (11)$$

**Table 1.** Table of specific conditions for COMSOL simulation.

Simulation Conditions	1	2	3	4
Heat Transfer Modes	Conduction	Conduction, convection coupling	Conduction, radiation coupling	Conduction, convection, and radiation coupling
Simplified Equation Conditions	Neglecting air flow, the base material's thermal conductivity is constant	Air is an ideal gas, neglecting viscous heating and work carried out by gas pressure	The surface of the pore is a diffuse gray surface that is not transparent, and the air inside the pore is an absolutely transparent medium that does not participate in radiative heat transfer	Simultaneously includes 2 and 3
COMSOL Physics Field Selection	Heat conduction in solids	Conjugate heat transfer (laminar)	Surface-to-surface radiative heat transfer Radiation properties are independent of wavelength; air transmittance is 1; the semi-cubic method is selected as the radiation calculation method; the radiation resolution is set to 256	Simultaneously includes 2 and 3
Main Parameters Setting for Physics Field	Solid 1 is set as the base material, solid 2 is set as air, and different thermal conductivity coefficients are assigned	Air undergoes compressible flow (Mach number less than 0.3), considering the effect of gravity, and pressure point constraints are set		Simultaneously includes 2 and 3
Field Variables	Temperature $T$	Temperature $T$ ; air flow velocity $u$ ; air pressure $p$	Temperature $T$	Temperature $T$ ; air flow velocity $u$ ; air pressure $p$
Temperature Difference ( $^{\circ}C$ )	40	40	40, 60, 80, 100, 120, 140	40

Formula (11) can be derived using Fourier's law, where  $k_i$  ( $i = 1, 2, 3, 4$ ) represents the effective thermal conductivity calculated under the  $i$ th condition ( $W/mK$ );  $a$  and  $b$  are the length and width of the specimen ( $\mu m$ ), respectively; and  $Q_{tot}$  is the total heat flux at the upper boundary of the specimen (J).

The simulation calculation flowchart is shown in Figure 4.

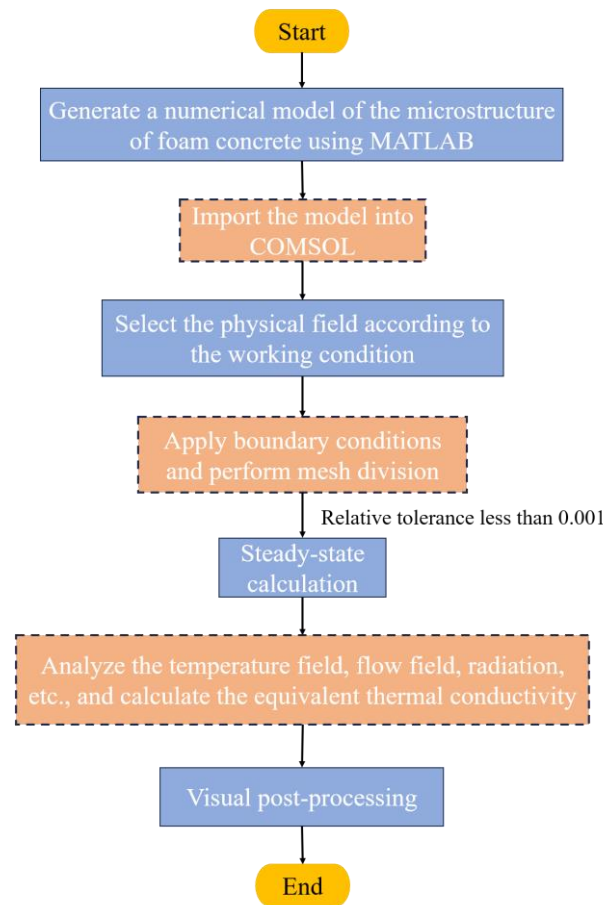


**Figure 4.** Flowchart of multi-physics coupled calculation.

The material parameters required for the simulation of the four operating conditions are listed in Table 2.

**Table 2.** Specific material parameters of COMSOL simulation.

Material Parameter	Matrix Thermal Conductivity $k_s$ (W/mK)	Surface Emissivity $\gamma$	Air Thermal Conductivity $k_g$ (W/mK)	Specific Heat Capacity of Air at Constant Pressure $c$ (J/kgK)	Aerodynamic Viscosity Coefficient $\mu$ (pa·s)	Air Density $\rho$ (kg/m <sup>3</sup> )
Relation to field variables	Constant	Constant	Functions of temperature	Functions of temperature	Functions of temperature	Function of temperature and pressure
Value	0.5	0.8	COMSOL Built-in Material Library Air	COMSOL Built-in Material Library Air	COMSOL Built-in Material Library Air	COMSOL Built-in Material Library Air

#### 4. Results Analysis

The microstructure parameters of foam concrete and the measured equivalent thermal conductivity values in this study are derived from the experiments conducted by She et al. [39]. He systematically characterized the microstructure of foam concrete and measured its equivalent thermal conductivity; the corresponding data are summarized in Table 3. This study validates the established model and calculation methods based on these experimental data and further investigates the heat transfer mechanism of foam concrete using numerical methods.

**Table 3.** Experimental data for foam concrete of different densities.

Number	Dry Density (kg/m <sup>3</sup> )	Porosity (%)	Average Pore Size (mm)	Mean Value $\mu$ ( $\mu\text{m}$ )	Standard Deviation $\sigma$ ( $\mu\text{m}$ )	Thermal Conductivity (W/mK)
1	1700	12	0.104	5.259	0.457	0.423
2	1500	21.39	0.113	5.312	0.323	0.363
3	1300	35.5	0.122	5.347	0.544	0.282
4	1000	47.24	0.173	5.514	0.465	0.217
5	800	59	0.263	5.693	0.235	0.165
6	600	69.22	0.59	6.132	0.342	0.124
7	500	75.45	0.7	6.232	0.343	0.091
8	400	79.19	0.8	6.587	0.212	0.08
9	300	84.17	0.956	6.952	0.122	0.065

#### 4.1. Model Validation

According to the microstructural parameters of foam concrete given in Table 3, a numerical model of foam concrete with a density of 800 kg/m<sup>3</sup> was established using the method in this study, under the condition of an overlap ratio of  $\delta = 0.2$ . Based on this, the equivalent thermal conductivity of the model was calculated according to working condition 1. Table 4 presents the results of three modeling and calculation iterations using the same parameters. As can be seen in Table 3, due to randomness, the porosity and calculated equivalent thermal conductivity of each modeling iteration are different, even with the same parameters, but the difference between the actual porosity and the expected porosity is very small. The equivalent thermal conductivity calculated in the three iterations is also relatively close to the results calculated in the literature [39], with a minimum error of 0 and a maximum error of 4.7%, but there is a 20% error compared to the measured values. To reduce the impact of random errors, the average value of the results from the three models is taken as the equivalent thermal conductivity of foam concrete under this parameter in the subsequent investigations in this study.

**Table 4.** COMSOL calculation results.

Number	Model Porosity (%)	$k_1$ (W/mK)	Average of $k_1$ (W/mK)	Calculated Value from Literature [39]	Experimental Value from Literature [39]
1	58.93	0.1322	0.1317	0.1346	0.165
2	59.06	0.1346			
3	58.99	0.1283			

To further verify the effectiveness of the method proposed in this study and to analyze the impact of the overlap ratio, numerical models of foam concrete with different densities were established based on the data in Table 2 for overlap ratios  $\delta = 0.1, 0.2,$  and  $0.4,$  respectively. The equivalent thermal conductivities of each model were then calculated according to working condition 1, and the calculated results were compared with the measured values and predicted values from other major analysis models. The results are shown in Figure 5.

From Figure 5, it can be seen that both the experimental values and the numerical simulation results of this study generally fall between the Maxwell–Eucken 1 model and the EMPT model, with the Maxwell–Eucken 1 model’s predictions significantly deviating from the actual values. Regardless of the model, the equivalent thermal conductivity significantly decreases with increasing porosity. This is because as the porosity increases, the proportion of the gas phase, which has a lower thermal conductivity, also increases, thus reducing the overall thermal conductivity. At the same porosity, as the overlap ratio  $\delta$  increases, the numerical simulation results of this study tend to decrease and approach

the EMPT model. This may be due to the increased overlap ratio causing more gas pores to merge, thereby reducing the solid phase conduction paths and lowering the equivalent thermal conductivity. The simulation results of this study are consistently lower than the experimental values; one possible reason is that condition 1 only considered thermal conduction and did not take into account thermal radiation and convection. When  $\delta = 0.1$ , the predictions of this study are always better than those of the EMPT model, close to the predictions of the Maxwell–Eucken 1 model at low porosities, and better than the Maxwell–Eucken 1 model at high porosities. However, when the porosity is between 30% and 70%, the predictions of the Maxwell–Eucken 1 model are optimal. Overall, the microstructural numerical model of this study is able to predict the equivalent thermal conductivity of foam concrete well over a wider range of porosities.

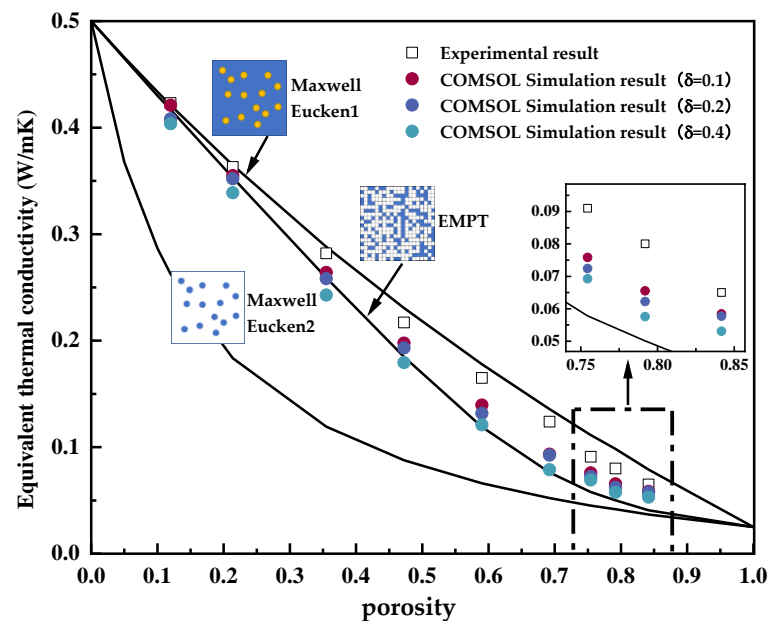


**Figure 5.** Comparison of COMSOL simulation results with experimental data and other analytical models.

#### 4.2. Conduction Heat Transfer Analysis

Under working condition 1, heat transfer analysis was performed on foam concrete with different densities using the microstructural numerical model, and the equivalent thermal conductivity  $k_1$  of the model was calculated and compared with the measured thermal conductivity  $k_{ex}$ . The curve of the ratio  $k_1/k_{ex}$  as a function of the density of foam concrete is shown in Figure 6. It can be seen in the figure that the smaller the overlap ratio, the larger the ratio and the smaller the error; the trends of the three curves are roughly the same, with the ratio decreasing and then increasing as the density increases. When the density is  $600 \text{ kg/m}^3$ , the ratio is the smallest and the error is the largest. Relatively speaking, at higher densities, the error in the model's predicted values is smaller.

The equivalent thermal conductivity can reflect the overall heat transfer performance of foam concrete, but it cannot reflect the details of heat transfer within foam concrete. With the help of a microstructural numerical model, the heat transfer situation inside foam concrete can be observed at the mesoscopic level.

Figure 7 shows the temperature contour maps and heat flux streamlines of foam concrete with three different densities:  $1700 \text{ kg/m}^3$ ,  $800 \text{ kg/m}^3$ , and  $500 \text{ kg/m}^3$ . As can be seen from the direction of the arrows in Figure 7, it can be seen that the heat flow tends to conduct through the matrix phase with a higher thermal conductivity, while avoiding conduction through the air phase with a lower thermal conductivity as much as possible. However, as the density decreases and the porosity increases, or as the overlap ratio increases and the number of interconnected pores increases, the optimal heat conduction

paths in the solid phase are obstructed, forcing the heat flow to conduct more through the gas phase. This also explains why the equivalent thermal conductivity of the foam concrete microstructural numerical model decreases with the increasing porosity or overlap ratio.

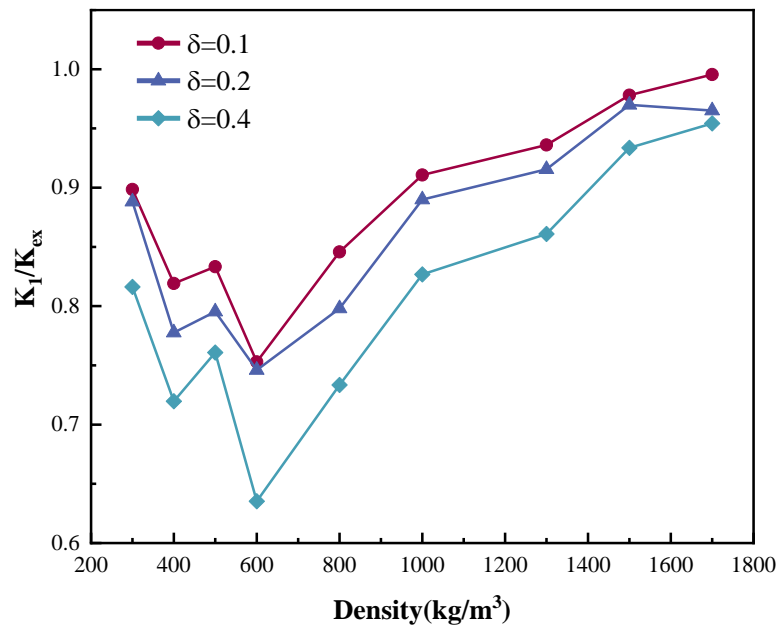


Figure 6. The ratio of the equivalent thermal conductivity  $k_1$  to the experimental value.

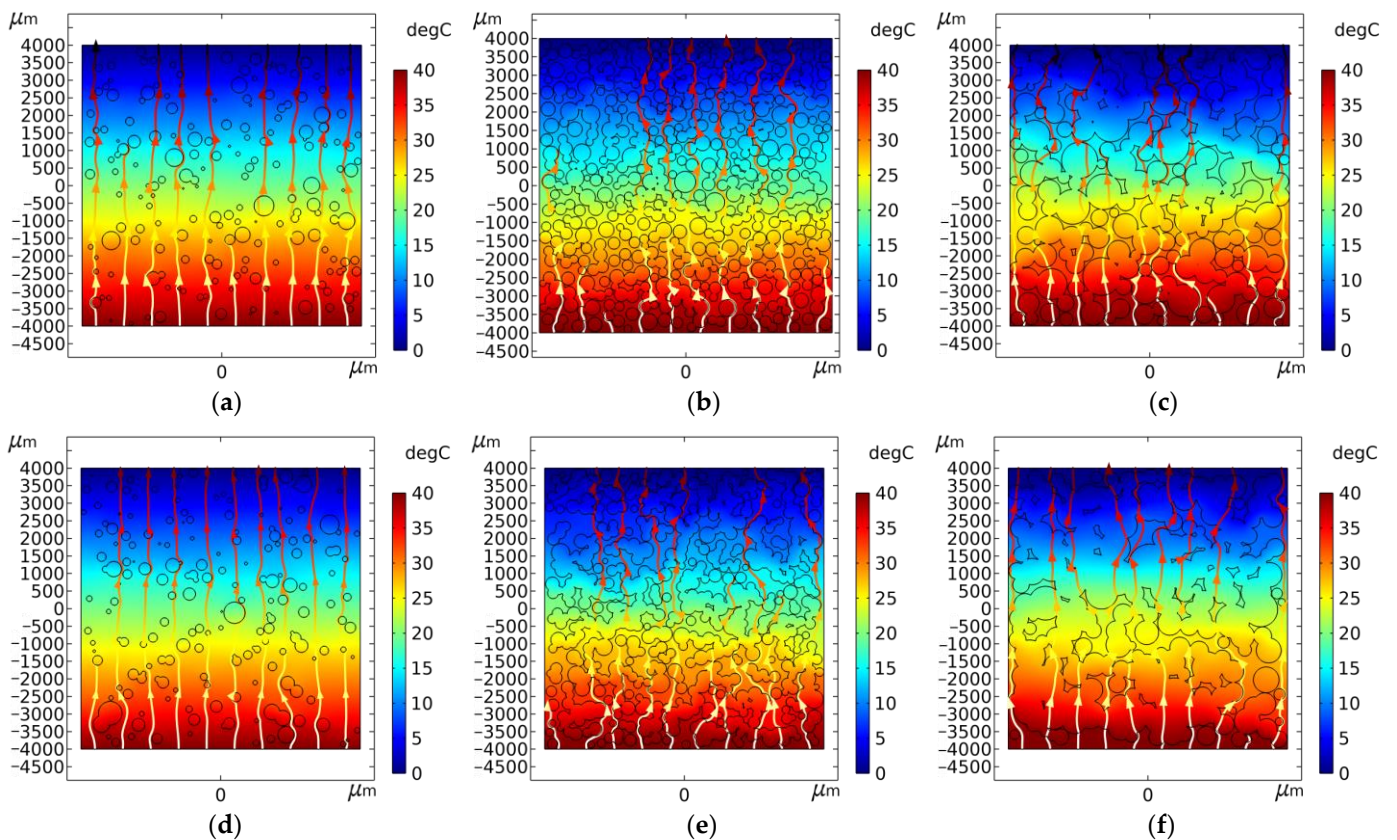
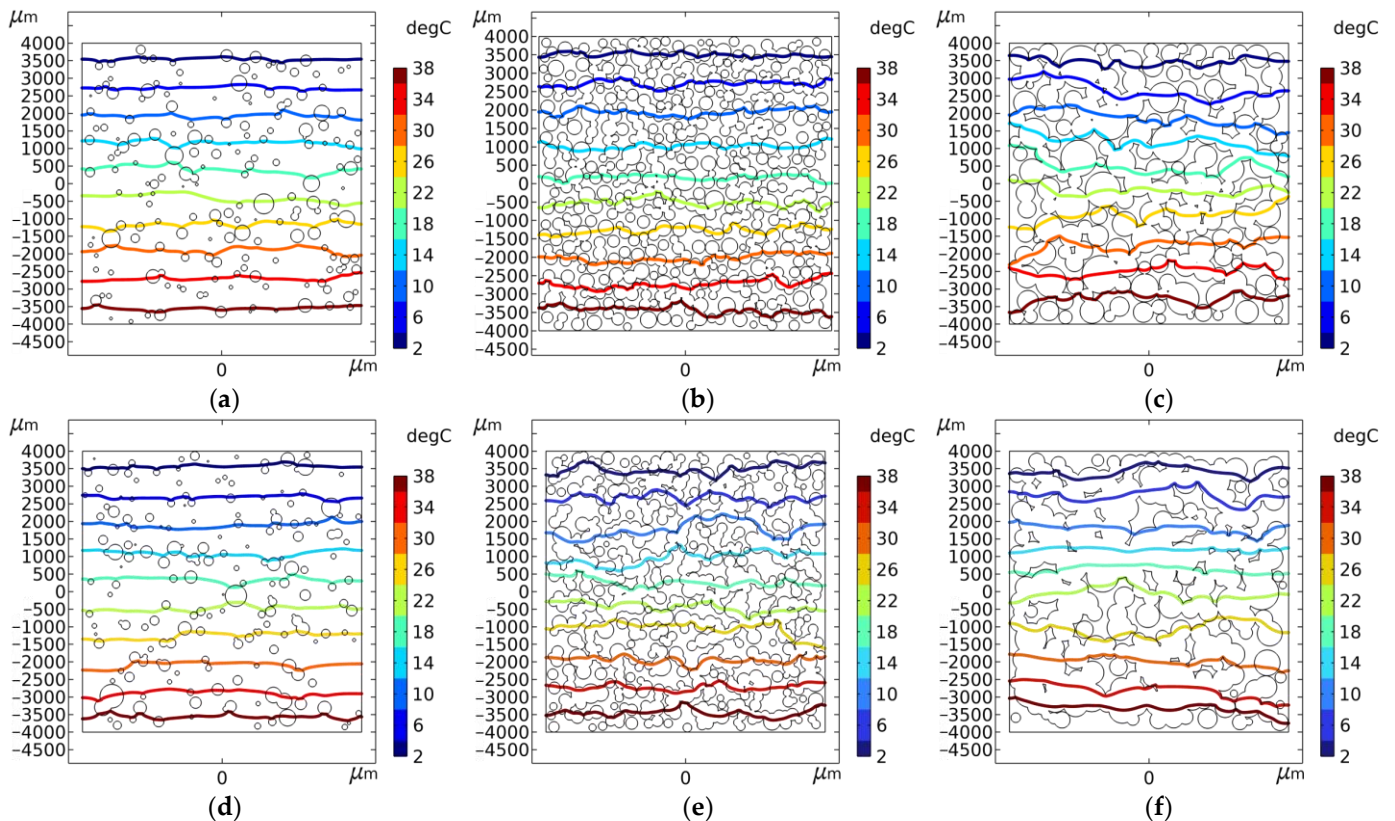


Figure 7. Temperature distribution and heat flux trend diagrams of foam concrete with different densities calculated using COMSOL simulation: (a) 1700 kg/m<sup>3</sup>,  $\delta = 0.1$ ; (b) 800 kg/m<sup>3</sup>,  $\delta = 0.1$ ; (c) 500 kg/m<sup>3</sup>,  $\delta = 0.1$ ; (d) 1700 kg/m<sup>3</sup>,  $\delta = 0.4$ ; (e) 800 kg/m<sup>3</sup>,  $\delta = 0.4$ ; (f) 500 kg/m<sup>3</sup>,  $\delta = 0.4$ .

Figure 8 further shows the isotherms of foam concrete with three different densities. As shown in the figure, regardless of the changes in density and overlap ratio, the isotherms are generally horizontally distributed, and the intervals are roughly the same, but the fluctuation amplitude of the isotherms varies to some extent. As the density decreases and the porosity increases, or as the overlap ratio increases and the number of interconnected pores increases, the fluctuation amplitude of the isotherms tends to increase, indicating that the non-uniformity of the temperature distribution inside the foam concrete is increasing.



**Figure 8.** Isotherms of foam concrete with different densities: (a)  $1700 \text{ kg/m}^3$ ,  $\delta = 0.1$ ; (b)  $800 \text{ kg/m}^3$ ,  $\delta = 0.1$ ; (c)  $500 \text{ kg/m}^3$ ,  $\delta = 0.1$ ; (d)  $1700 \text{ kg/m}^3$ ,  $\delta = 0.4$ ; (e)  $800 \text{ kg/m}^3$ ,  $\delta = 0.4$ ; (f)  $500 \text{ kg/m}^3$ ,  $\delta = 0.4$ .

In the conductive heat transfer analysis, the impact of the different overlap ratio parameters on heat transfer was investigated. For simplicity, in the subsequent coupled heat transfer analysis, only an overlap ratio of  $\delta = 0.4$  was considered for this study.

#### 4.3. Conduction and Convection Coupled Heat Transfer Analysis

Taking foam concrete with densities of  $800 \text{ kg/m}^3$  and  $500 \text{ kg/m}^3$  as examples, and, considering the coupling of conduction and convection, the heat transfer situation inside the foam concrete was analyzed using a microstructure numerical model.

Figure 9 shows the isotherm diagram under the coupling of conduction and convection. Compared with the isotherm in Figure 8e,f, which considers only conduction, it can be seen that the difference in temperature distribution inside the foam concrete under the two conditions is very small.

Figure 10 shows the velocity contour of the air in the pores of the foam concrete. It can be seen in the figure that as the pore size increases, the velocity of the air in the pores increases, but the absolute value of the velocity is small. When the density is  $500 \text{ kg/m}^3$ , the calculated Reynolds number  $R_e \approx 10^{-3} \ll 1$ , which means that the viscous force is much greater than the inertial force when the air flows and that the convective heat transfer effect of the air is weak.

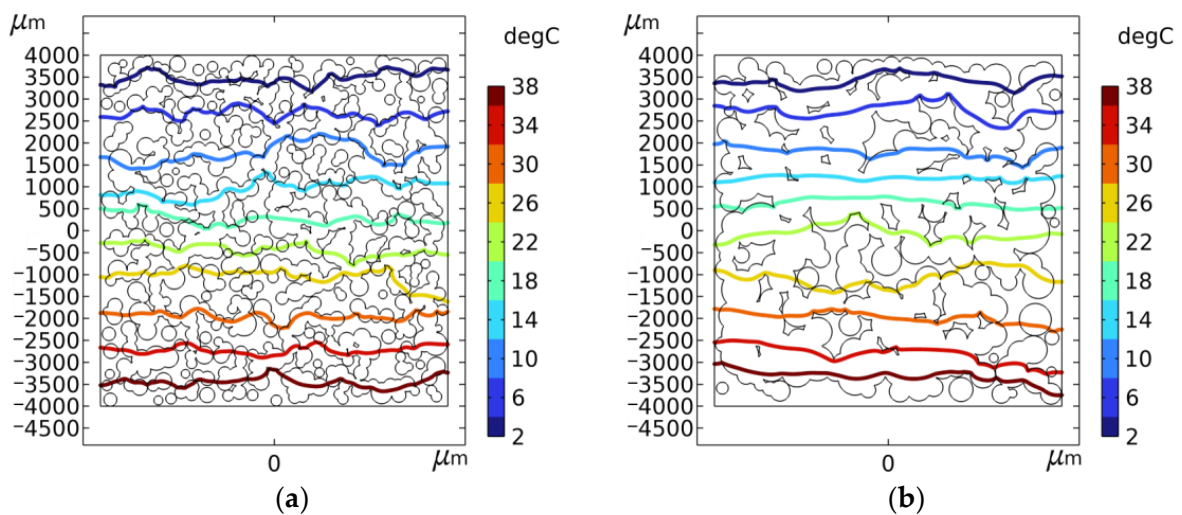


Figure 9. Isotherms of foam concrete with different densities: (a)  $800 \text{ kg/m}^3$ ; (b)  $500 \text{ kg/m}^3$ .

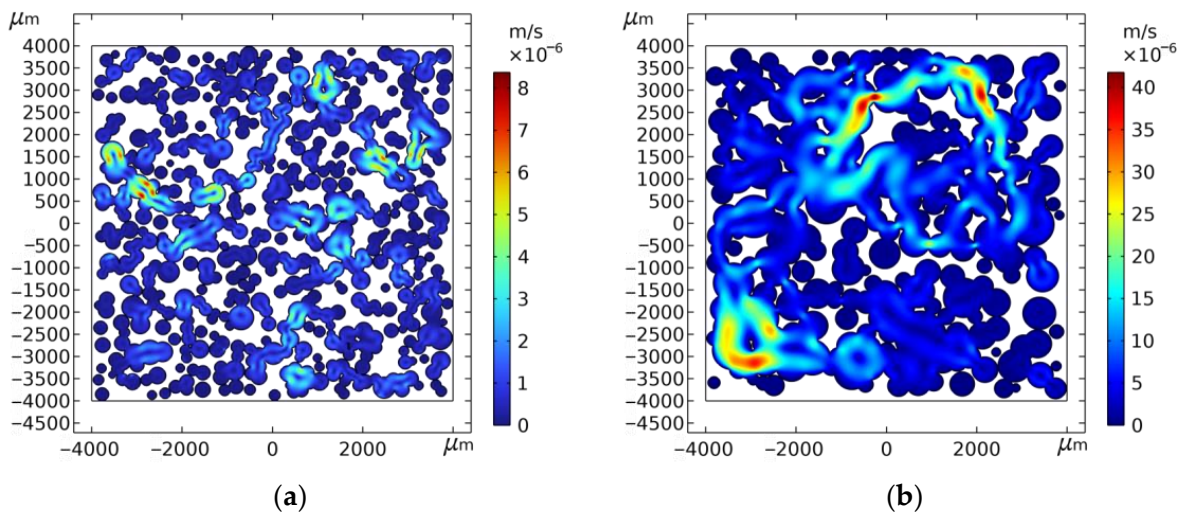
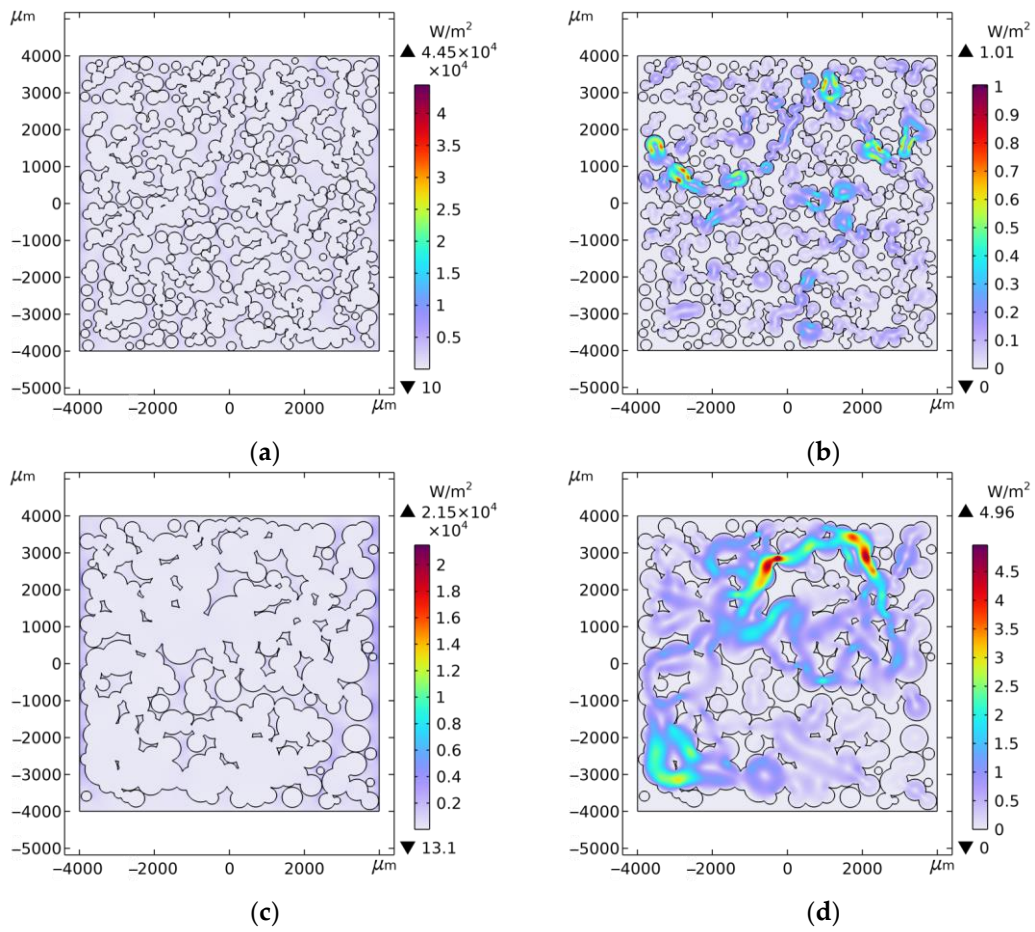


Figure 10. Internal velocity clouds for foam concrete with different densities: (a)  $800 \text{ kg/m}^3$ ; (b)  $500 \text{ kg/m}^3$ .

Under the coupling of convection and conduction, the total heat flux equals the sum of the conductive heat flux and the convective heat flux. Figure 11 shows the cloud of the conductive heat flux and the convective heat flux in the foam concrete, respectively. It can be observed in the figure that as the pore size increases, the convective heat flux remains much smaller than the conductive heat flux, even though the convective heat flux increases and the conductive heat flux decreases. This indicates that under condition 2, heat transfer in foam concrete is dominated by conduction, with a relatively minor influence from convection.

Figure 12 further presents the ratio of the equivalent thermal conductivity  $k_2$  under condition 2 to the equivalent thermal conductivity  $k_1$  under condition 1 for foam concrete with different densities. It can be seen in the figure that regardless of the change in density,  $k_2/k_1$  is always close to 1, indicating that the contribution of convective heat transfer in actual foam concrete is very small. This is due to the pore size of foam concrete being less than 1 mm, which restricts the convective effect of the gas in the pores [40].



**Figure 11.** Heat flux clouds for foam concrete with different densities: (a) 800 kg/m<sup>3</sup>—conductive heat flux; (b) 800 kg/m<sup>3</sup>—convective heat flux; (c) 500 kg/m<sup>3</sup>—conductive heat flux; (d) 500 kg/m<sup>3</sup>—convective heat flux.

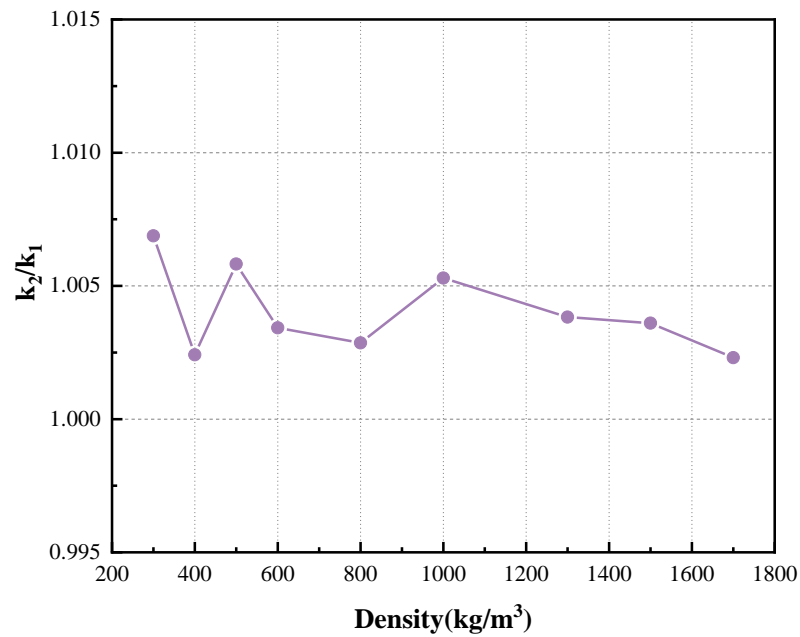


**Figure 12.** The variation in the ratio of the equivalent thermal conductivity calculated under condition 2 to that calculated under condition 1 with the density of foam concrete.

Related studies have shown that the influence of convective heat transfer needs to be considered only when the pore size of the porous medium is greater than 4 mm. To further verify this conclusion, numerical methods are used for simulation studies. For simplicity, it is assumed that the standard deviation of the pore size and the overlap rate are both zero, the porosity of the model is 50%, and the temperature difference between the upper and lower edges is 40 °C. When the pore size changes, the equivalent thermal conductivity of the model under condition 1 and condition 2 is calculated. The results are listed in Table 5. It can be seen in the table that when the pore size is greater than 14 mm, the contribution of the convective heat transfer significantly increases.

**Table 5.** Equivalent thermal conductivity for different pore sizes.

Pore Size	2 mm	4 mm	6 mm	8 mm	10 mm	12 mm	14 mm	16 mm
$k_1$	0.1715	0.1667	0.1620	0.1759	0.1764	0.1690	0.1467	0.1158
$k_2$	0.1739	0.1696	0.1634	0.1773	0.1778	0.1713	0.1563	0.1431
$k_1/k_2$	1.014	1.017	1.009	1.008	1.008	1.014	1.065	1.236

The air velocity in the models with pore sizes of 4 mm and 14 mm is shown in Figure 13 under condition 2. It can be seen in the figure that with the increase in pore size, the velocity increases by two orders of magnitude. The isotherms of these two pore size models under condition 1 and condition 2 are shown in Figure 14. It can be seen in the figure that when the pore size is 4 mm, the isotherms under the two conditions are basically the same, indicating that the convective effect is not significant. At this time, the calculated Reynolds number  $R_e \approx 0.1$  and the Rayleigh number  $R_a \approx 20$ , while, when the pore size is 14 mm, the isotherms of the matrix part under the two conditions are basically the same, but the isotherms inside the pores are quite different: condition 2 shows more fluctuations compared to condition 1; this is caused by the significant convective effect. At this time, the calculated Reynolds number  $R_e \approx 22$  and the Rayleigh number  $R_a \approx 3000$ . The studies in the literature [43] suggest that the convective effect becomes significant when the Rayleigh number  $R_a$  is at least greater than 1000, which is consistent with the simulation results of this study.

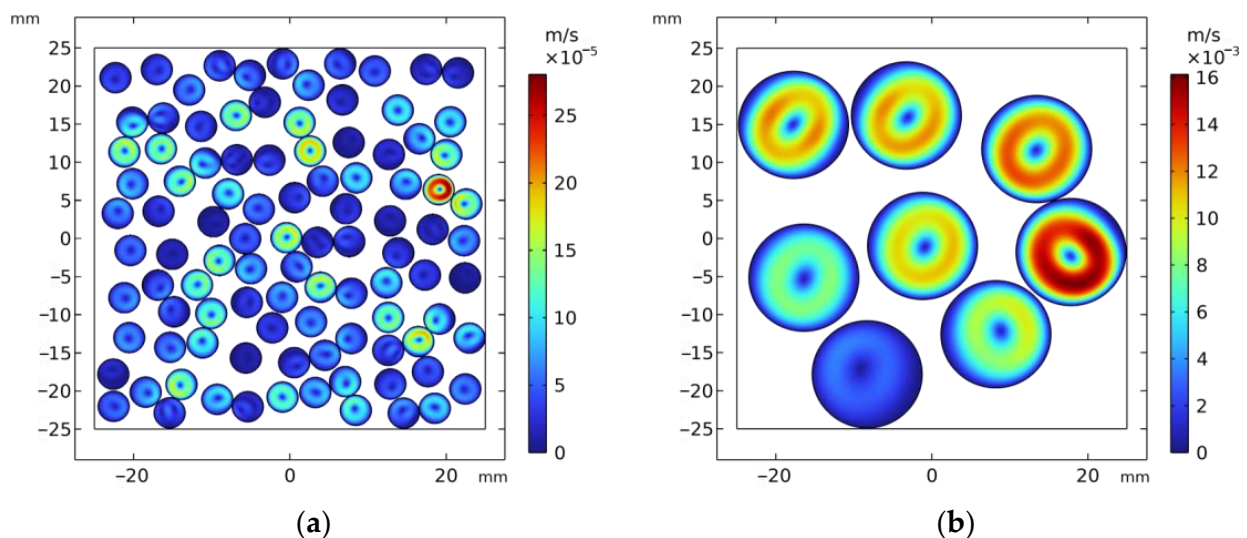


**Figure 13.** Internal velocity cloud map of foam concrete with different pore sizes: (a)  $d = 4$  mm; (b)  $d = 14$  mm.

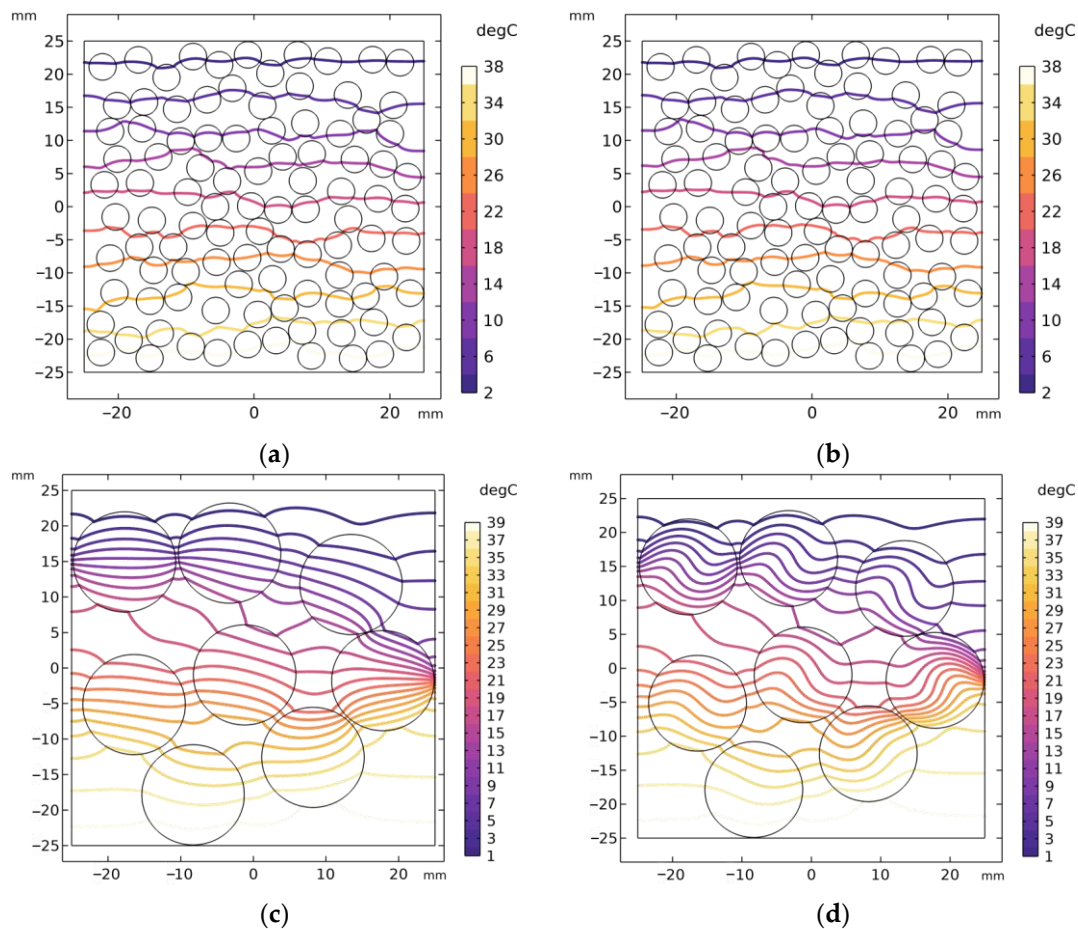


**Figure 14.** The isotherms of foam concrete with different pore sizes under different operating conditions: (a) 4 mm—condition 1; (b) 4 mm—condition 2; (c) 14 mm—condition 1; (d) 14 mm—condition 2.

#### 4.4. Conduction and Radiation Coupled Heat Transfer Analysis

Taking foam concrete with densities of  $800 \text{ kg/m}^3$  and  $500 \text{ kg/m}^3$  as an example, the heat transfer inside the foam concrete was analyzed using a microstructure numerical model under condition 3. Figure 15 shows the contour maps of conductive heat flux and radiative heat flux in foam concrete with a temperature difference of  $40 \text{ }^\circ\text{C}$ . It can be seen in the figure that as the density decreases and the pore size increases, the conductive heat flux decreases while the radiative heat flux increases. The maximum value of the conductive heat flux is approximately  $10^3$  times that of the maximum value of the radiative heat flux, indicating that the radiative heat flux is still a small quantity compared to the conductive heat flux. However, comparing Figure 11b with Figures 15b and 11d with Figure 15d, it can be seen that under the same conditions, the maximum value of the radiative heat flux is more than 10 times that of the maximum value of the convective heat flux, indicating that the impact of radiation in foam concrete is higher than that of convection.

Figure 16 shows the ratio of the equivalent thermal conductivity  $k_3$  under condition 3 to the equivalent thermal conductivity  $k_1$  under condition 1 for foam concrete with different densities at a temperature difference of  $40 \text{ }^\circ\text{C}$ . It can be seen in the figure that  $k_3/k_1$  increases continuously as the density decreases. When the density is greater than  $1000 \text{ kg/m}^3$ ,  $k_3/k_1$  is close to 1, indicating that the contribution of radiative heat transfer is not significant for high-density foam concrete. However, when the density is less than  $600 \text{ kg/m}^3$ ,  $k_3/k_1$  increases rapidly, indicating that the contribution of radiative heat transfer increases rapidly at this point; thus, the impact of radiative heat transfer cannot be ignored for low-density foam concrete.

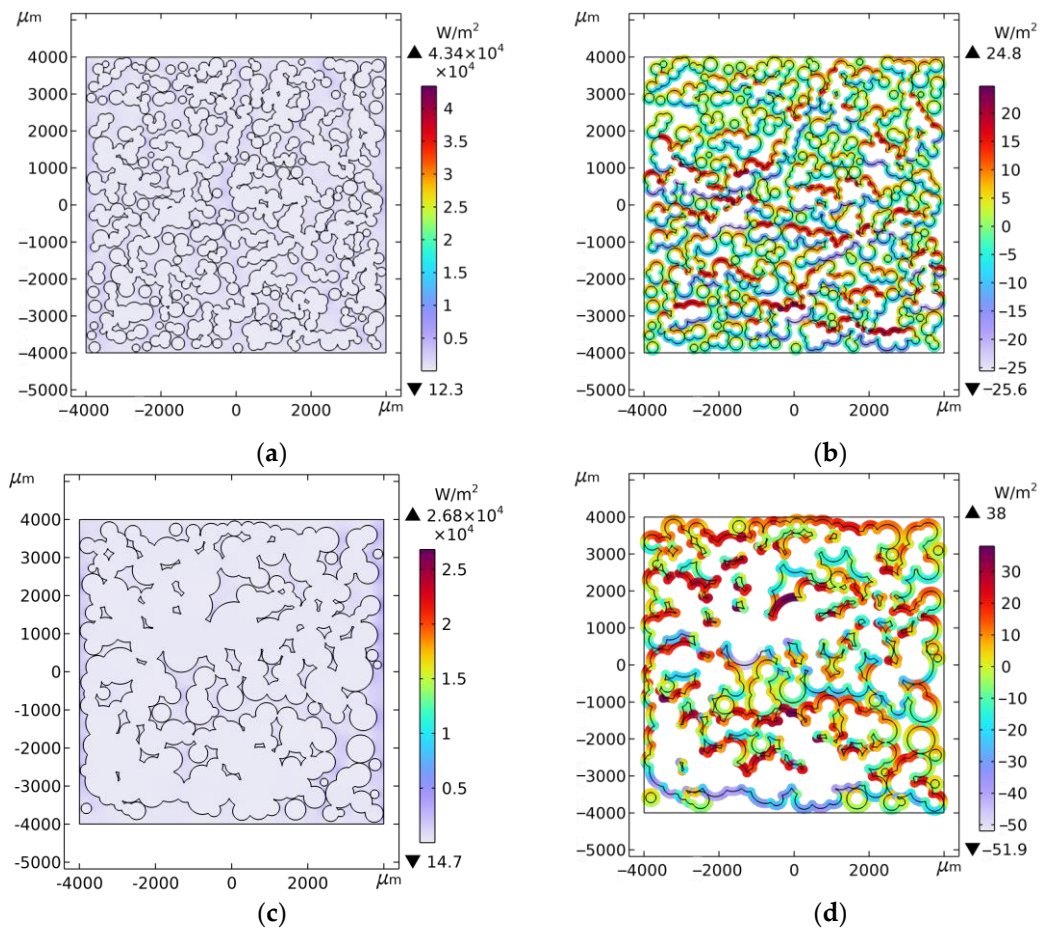


**Figure 15.** Heat flux clouds for foam concrete with different densities: (a) 800 kg/m<sup>3</sup>—conductive heat flux; (b) 800 kg/m<sup>3</sup>—radiative heat flux; (c) 500 kg/m<sup>3</sup>—conductive heat flux; (d) 500 kg/m<sup>3</sup>—radiative heat flux.

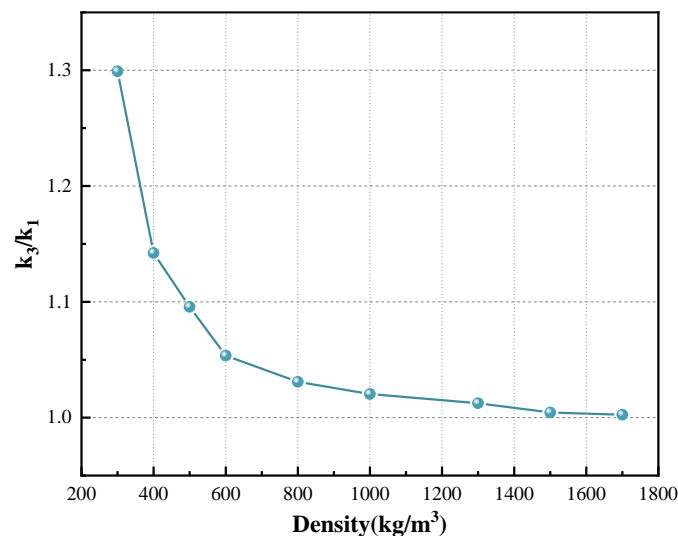


**Figure 16.** The variation in the ratio of the equivalent thermal conductivity calculated under condition 3 to that calculated under condition 1 with the density of foam concrete.

The Stefan–Boltzmann law states that the higher the temperature of an object, the stronger its radiative ability, and the radiative ability of an object is directly proportional to the fourth power of its temperature. Therefore, when analyzing the radiative heat transfer

of foam concrete, the temperature difference is also a very important factor. Figure 17 further shows the radiative heat flux of foam concrete with densities of  $800 \text{ kg/m}^3$  and  $500 \text{ kg/m}^3$  under temperature differences of  $80 \text{ }^\circ\text{C}$  and  $120 \text{ }^\circ\text{C}$ , respectively. It can be seen in the figure that as the temperature difference increases, the radiative heat flux in the foam concrete significantly increases.

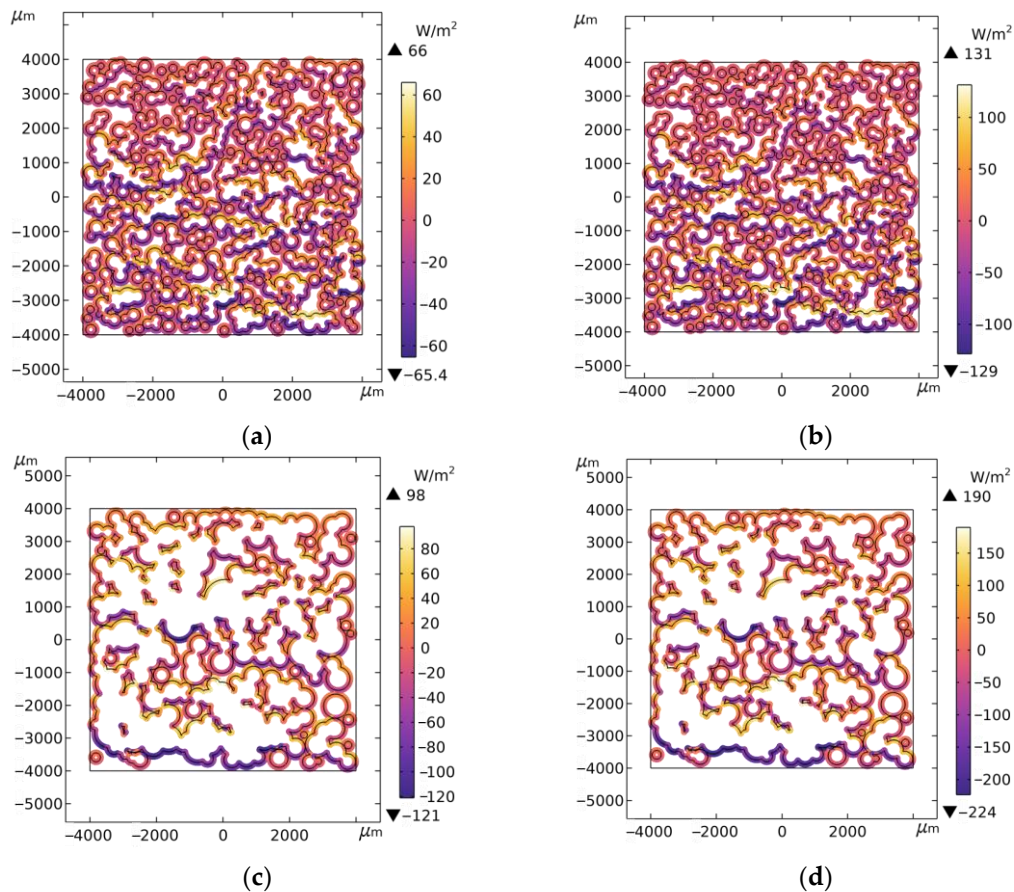


**Figure 17.** Radiative heat flux clouds for foam concrete with densities of  $500 \text{ kg/m}^3$  and  $800 \text{ kg/m}^3$  under different temperature differences: (a)  $800 \text{ kg/m}^3$ ,  $\Delta T = 80 \text{ }^\circ\text{C}$ ; (b)  $800 \text{ kg/m}^3$ ,  $\Delta T = 120 \text{ }^\circ\text{C}$ ; (c)  $500 \text{ kg/m}^3$ ,  $\Delta T = 80 \text{ }^\circ\text{C}$ ; (d)  $500 \text{ kg/m}^3$ ,  $\Delta T = 120 \text{ }^\circ\text{C}$ .

Figure 18 further shows the curve of the equivalent thermal conductivity of foam concrete as a function of the temperature difference. It can be seen in the figure that under condition 1, the equivalent thermal conductivity  $k_1$  does not change with the temperature difference, while under condition 3, the equivalent thermal conductivity  $k_3$  increases with the increase in temperature difference, and  $k_3$  is approximately linearly related to the temperature difference, with the slope increasing as the density of foam concrete decreases. Chao Fan et al. [43] found a similar phenomenon as well. The equivalent thermal conductivity  $k_3$  can be thought of as consisting of two parts: the first part is  $k_1$ , representing the thermal conductivity contributed by conduction, and  $k_1/k_3$  represents the proportion of the conduction contribution; the second part is  $k_3 - k_1$ , representing the thermal conductivity contributed by radiation, and  $(k_3 - k_1)/k_3$  represents the proportion of the radiation contribution. Under condition 3, the curves of the percentage contributions of radiation and conduction as a function of the temperature difference are shown in Figure 19. It can be seen in the figure that at the same density, the greater the temperature difference, the greater the contribution of radiation, and the smaller the contribution of conduction; at the same temperature difference, the smaller the density, the greater the contribution of radiation and the smaller the contribution of conduction. Within the

considered range of temperature differences, heat transfer in foam concrete is always dominated by conduction.

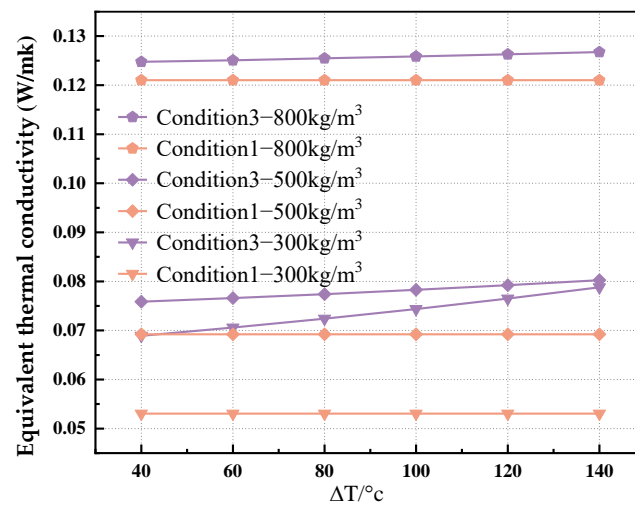


Figure 18. The influence of temperature difference on the equivalent thermal conductivity.

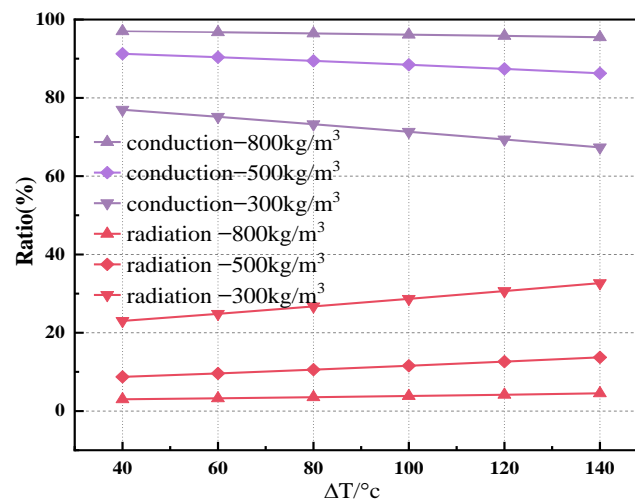
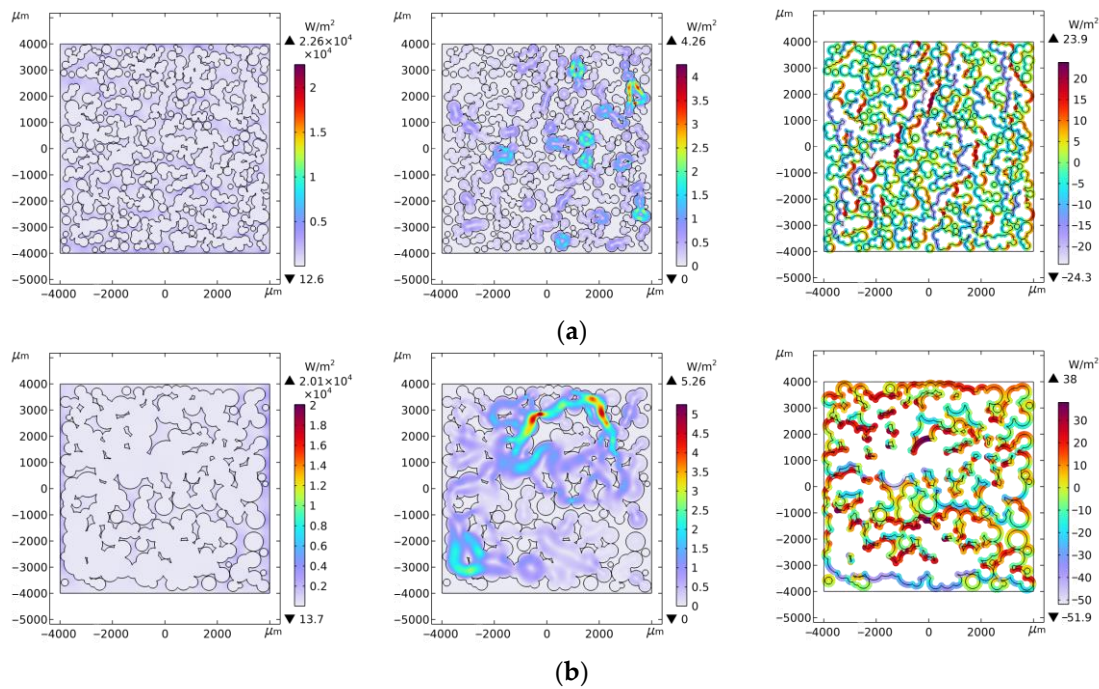


Figure 19. The variation of radiation and conduction contribution ratios with temperature difference.

#### 4.5. Conduction, Convection, and Radiation Coupled Heat Transfer Analysis

When the temperature difference is 40 °C, under condition 4, the cloud of conductive heat flux, convective heat flux, and radiative heat flux for foam concrete with densities of 800 kg/m<sup>3</sup> and 500 kg/m<sup>3</sup> are as presented in Figure 20. Compared with conditions 2 and 3, there is no order of magnitude change in the size of the three types of heat flux. Looking at the maximum values of the heat fluxes, the radiation is approximately 10 times that of the convection, and the conduction is approximately 10,000 times that of the convection. The analysis of heat fluxes shows that in the heat transfer of foam concrete, conduction plays a dominant role, the impact of convection is smaller, and the influence of radiation is greater than that of convection.

For foam concrete with different densities and a temperature difference of 40 °C, Figure 21 shows the curves of the ratio  $k_4/k_3$  and the ratio  $k_4/k_2$  as a function of density. It can be seen in the figure that the value of  $k_4/k_3$  is very close to 1, indicating that convection has a small impact on the heat transfer of foam concrete. The trend of  $k_4/k_2$  is basically consistent with the trend of  $k_3/k_1$  in Figure 16, indicating that radiation has a certain impact on the heat transfer of foam concrete and that the lower the density of the foam concrete, the greater the impact of radiative heat transfer.



**Figure 20.** Heat flux clouds for foam concrete with different densities (a) 800 kg/m<sup>3</sup>; (b) 500 kg/m<sup>3</sup>. (Left, middle, and right represent conduction, convection, and radiation, respectively).

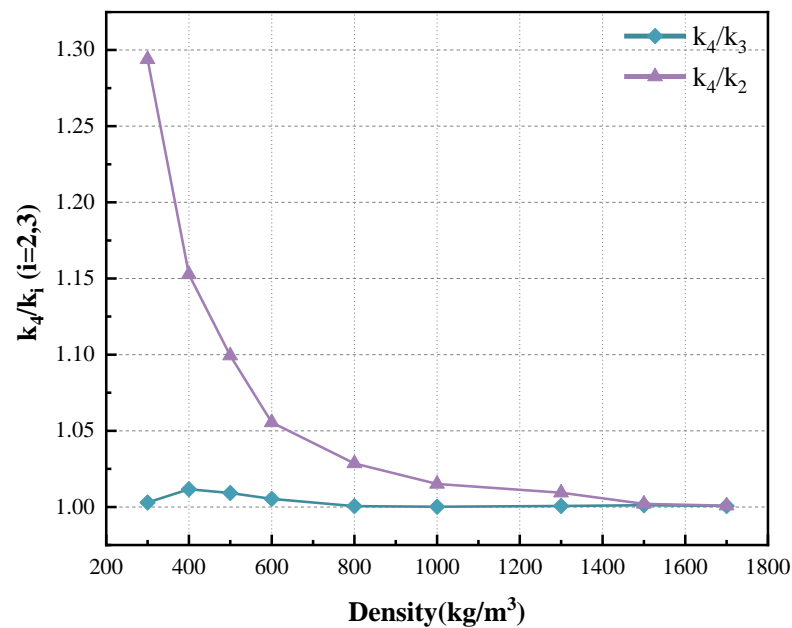


**Figure 21.** The variation in the ratio of the equivalent thermal conductivity calculated under condition 4 to that calculated under conditions 2 and 3 with the density of foam concrete.

To further analyze the contributions of conduction, convection, and radiation to the heat transfer of foam concrete, the equivalent thermal conductivity  $k_4$  can be simply considered as consisting of three parts: the first part is  $k_1$ , representing the thermal conductivity contributed by conduction; the second part is  $k_4 - k_3$ , representing the thermal conductivity contributed by convection; and the third part is  $k_4 - k_2$ , representing the thermal conductivity contributed by radiation. The curves of the ratio of each part to  $k_4$  as a function of density are all plotted in Figure 22. It can be seen in the figure that regardless of the density of foam concrete, the impact of convection is negligible; as the density decreases, the impact of conduction shows a downward trend, while the impact of radiation shows an upward

trend, and when the density is less than  $1000 \text{ kg/m}^3$ , this change accelerates. When the density is  $300 \text{ kg/m}^3$ , the contribution of radiation exceeds 20%, while the contribution of conduction is less than 80%, indicating that the impact of radiation on heat transfer cannot be ignored for low-density foam concrete.

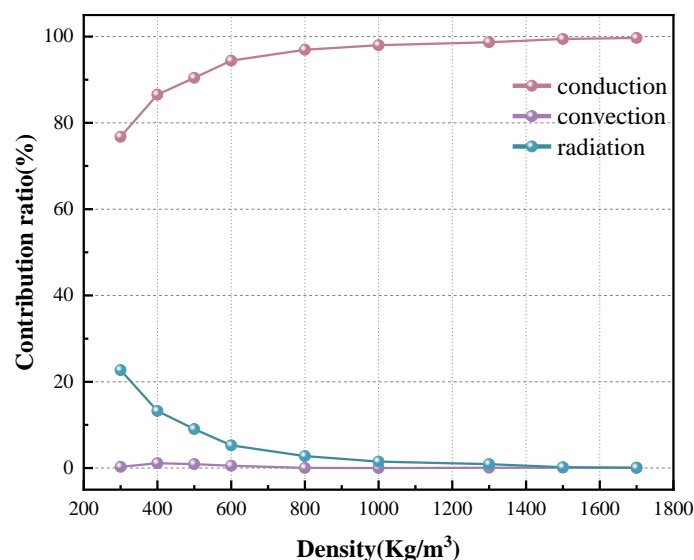


**Figure 22.** The variation in conduction, convection, and radiation ratio with density.

When the temperature difference is  $40 \text{ }^\circ\text{C}$ , the ratios of the equivalent thermal conductivity calculated for each condition to the experimental results are plotted as a function of density, as shown in Figure 23. It can be seen in the figure that under condition 1 (considering only conduction), the simulation values are always smaller than the experimental values, and the error in the simulation results is relatively small in the high-density range, while it is relatively large in the medium and low-density range. As the impact of convective heat transfer in foam concrete is very small, the simulation results under condition 2 (coupling of conduction and convection) are close to those under condition 1, indicating that considering convective heat transfer does not significantly reduce the simulation error. Under condition 3 (coupling of conduction and radiation), due to the contribution of radiative heat transfer, the equivalent thermal conductivity is increased compared to conditions 1 and 2, resulting in simulation results that are closer to the measured values, especially for low-density foam concrete, where the impact of radiative heat transfer is greater and the improvement in the simulation results is more pronounced. Condition 4 considers conduction, convection, and radiation comprehensively, and the simulation results are similar to those under condition 3 but closer to the measured values, especially for foam concrete with densities of  $400 \text{ kg/m}^3$ ,  $500 \text{ kg/m}^3$ , and  $600 \text{ kg/m}^3$ , where the improvement in the simulation results is more noticeable.

#### 4.6. Potential Applications and Developments

This study proposed a method for simulating the heat transfer behavior of foam concrete under multiple working conditions and analyzed the heat transfer patterns of foam concrete under different modes of heat transfer. The limitation of the research method in this study lies in the fact that the equivalent thermal conductivity of foam concrete calculated by the two-dimensional numerical model is smaller than the experimental results. This is because the two-dimensional model neglects the heat transfer path in the third spatial direction. Therefore, the method for generating foam concrete microstructure in this study can be extended to three-dimensional space to more accurately study the heat transfer performance of foam concrete materials. On the other hand, building envelope structures made of foam concrete can provide thermal insulation. Combining the thermal performance of foam concrete external walls with the main building can improve the

thermal insulation performance of the external walls, enhance the living comfort of the building, and promote energy conservation and environmental protection, all of which are of great significance.

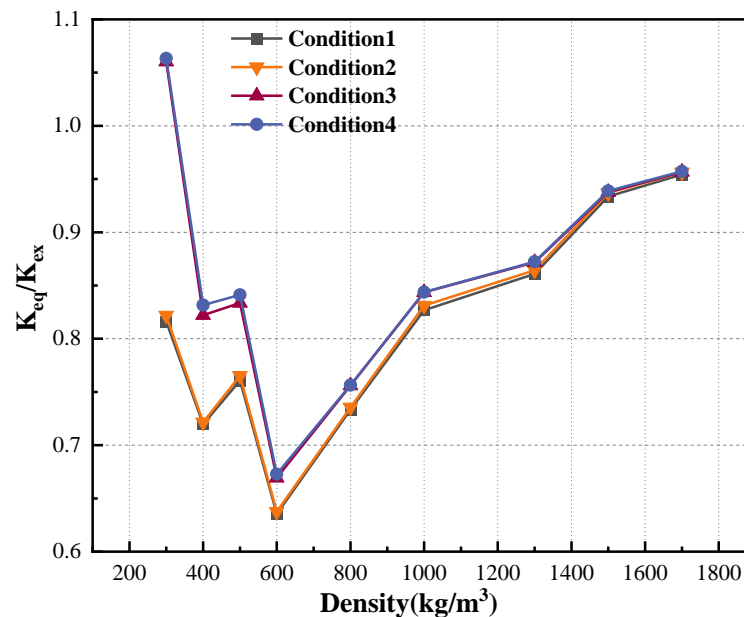


**Figure 23.** The ratio of the equivalent thermal conductivity calculated under the four conditions to the experimental value.

## 5. Conclusions

Based on the statistical parameters of the pore structure of foam concrete, this study proposes a random numerical modeling method, uses this method to establish a microstructure numerical model of foam concrete, and analyzes the heat transfer mechanism of foam concrete from a mesoscopic level with the help of this model. By comparing four different conditions, the influence of conduction, convection, and radiation on the heat transfer of foam concrete is analyzed, and the contribution rates of conduction, convection, and radiation in the heat transfer of foam concrete are quantitatively analyzed using the equivalent thermal conductivity.

From a mesoscopic scale, it was observed that as the porosity and overlap ratio increase, the optimal conduction paths in the solid phase are blocked, the heat transfer distance is extended, and the effective thermal conductivity of the foam concrete significantly decreases. The impact of convection is negligible because the maximum pore size in foam concrete is less than 1 mm, and the small space restricts the convection of gas. The simulation study in this paper shows that a noticeable convective effect only appears in foam concrete when the pore size is greater than 12 mm. The contribution of radiation is related not only to the density (porosity) of the foam concrete but also to the temperature difference. The lower the density, the greater the contribution of radiation. When the density is 300 kg/m<sup>3</sup>, the contribution ratio of the radiation even exceeds 20%. On the other hand, the greater the temperature difference, the greater the contribution of radiation. The contribution of radiation is approximately linearly related to the temperature difference.

Conduction plays a dominant role in the heat transfer of foam concrete. For high-density foam concrete ( $\rho \geq 1000$ ), due to the small pore size and low porosity, the impact of convection and radiation is minimal, and the contribution of conduction is close to 100%. However, as the density decreases, the contribution of conduction shows a decreasing trend due to the gradually increasing impact of radiation. When the density is 300 kg/m<sup>3</sup>, the contribution rate of conduction is below 80%. Despite this, conduction still holds an absolute dominant position in the heat transfer of foam concrete.

**Author Contributions:** Conceptualization, T.H. and M.W.; methodology, T.H. and M.W.; software, T.H. and M.W.; validation, T.H., M.W. and S.F.; formal analysis, T.H. and M.W.; investigation, M.W.; resources, M.W., Z.P., X.H. and Y.S.; data curation, M.W., S.F., Z.P., X.H. and Y.S.; writing—original draft preparation, T.H. and M.W.; writing—review and editing, T.H., S.F., Z.P., X.H. and Y.S.; visualization, M.W., S.F., Z.P., X.H. and Y.S.; supervision, T.H., S.F., Z.P., X.H. and Y.S.; project administration, M.W., S.F., Z.P., X.H. and Y.S.; funding acquisition, T.H. All authors have read and agreed to the published version of the manuscript.

**Funding:** This research received no external funding.

**Data Availability Statement:** The data used in the article can be obtained from the author here.

**Acknowledgments:** The authors would like to acknowledge the Hubei University of Technology.

**Conflicts of Interest:** The authors declare no conflicts of interest.

## References

1. Sadineni, S.B.; Madala, S.; Boehm, R.F. Passive Building Energy Savings: A Review of Building Envelope Components. *Renew. Sustain. Energy Rev.* **2011**, *15*, 3617–3631. [[CrossRef](#)]
2. Li, T.; Zhu, M.; Yang, Z.; Song, J.; Dai, J.; Yao, Y.; Luo, W.; Pastel, G.; Yang, B.; Hu, L. Wood Composite as an Energy Efficient Building Material: Guided Sunlight Transmittance and Effective Thermal Insulation. *Adv. Energy Mater.* **2016**, *6*, 1601122. [[CrossRef](#)]
3. Cao, M.; Liu, B.-W.; Zhang, L.; Peng, Z.-C.; Zhang, Y.-Y.; Wang, H.; Zhao, H.-B.; Wang, Y.-Z. Fully Biomass-Based Aerogels with Ultrahigh Mechanical Modulus, Enhanced Flame Retardancy, and Great Thermal Insulation Applications. *Compos. Part B Eng.* **2021**, *225*, 109309. [[CrossRef](#)]
4. Zhou, H.; Zhao, X.; Wang, X.; Song, T.; Liu, H.; Zhang, H. Elevated Temperature Properties of Foam Concrete: Experimental Study, Numerical Simulation, and Theoretical Analysis. *Constr. Build. Mater.* **2024**, *411*, 134393. [[CrossRef](#)]
5. Briga-Sá, A.; Nascimento, D.; Teixeira, N.; Pinto, J.; Caldeira, F.; Varum, H.; Paiva, A. Textile Waste as an Alternative Thermal Insulation Building Material Solution. *Constr. Build. Mater.* **2013**, *38*, 155–160. [[CrossRef](#)]
6. Korjenic, A.; Petránek, V.; Zach, J.; Hroudová, J. Development and Performance Evaluation of Natural Thermal-Insulation Materials Composed of Renewable Resources. *Energy Build.* **2011**, *43*, 2518–2523. [[CrossRef](#)]
7. Zhao, W.; Zhao, H.-B.; Cheng, J.-B.; Li, W.; Zhang, J.; Wang, Y.-Z. A Green, Durable and Effective Flame-Retardant Coating for Expandable Polystyrene Foams. *Chem. Eng. J.* **2022**, *440*, 135807. [[CrossRef](#)]
8. Chattopadhyay, D.K.; Webster, D.C. Thermal Stability and Flame Retardancy of Polyurethanes. *Prog. Polym. Sci.* **2009**, *34*, 1068–1133. [[CrossRef](#)]
9. Luo, Y.; Li, Q.; Jiang, L.; Zhou, Y. Analysis of Chinese Fire Statistics during the Period 1997–2017. *Fire Saf. J.* **2021**, *125*, 103400. [[CrossRef](#)]
10. Fei, Y.; Shun-Bing, Z.; Xue-Feng, H. Analysis and Flame Retarding Design of Combustibles in Nanjing Typical Historical Buildings. *Procedia Eng.* **2011**, *11*, 625–633. [[CrossRef](#)]
11. Khan, A.A.; Khan, M.A.; Domada, R.V.V.; Huang, X.; Usmani, A.; Bakhtiyari, S.; Ashtiani, M.J.; Garivani, S.; Aghakouchak, A.A. Fire Modelling Framework for Investigating Tall Building Fire: A Case Study of the Plasco Building. *Case Stud. Therm. Eng.* **2023**, *45*, 103018. [[CrossRef](#)]
12. Priyatham, B.P.R.V.S.; Lakshmayya, M.T.S.; Chaitanya, D.V.S.R.K. Review on Performance and Sustainability of Foam Concrete. *Mater. Today Proc.* **2023**, S2214785323019788. [[CrossRef](#)]
13. Wang, X.; Liu, L.; Zhou, H.; Song, T.; Qiao, Q.; Zhang, H. Improving the Compressive Performance of Foam Concrete with Ceramsite: Experimental and Meso-Scale Numerical Investigation. *Mater. Des.* **2021**, *208*, 109938. [[CrossRef](#)]
14. Ducman, V.; Korat, L. Characterization of Geopolymer Fly-Ash Based Foams Obtained with the Addition of Al Powder or H<sub>2</sub>O<sub>2</sub> as Foaming Agents. *Mater. Charact.* **2016**, *113*, 207–213. [[CrossRef](#)]
15. Mobaraki, B.; Ma, H.; Lozano Galant, J.A.; Turmo, J. Structural Health Monitoring of 2D Plane Structures. *Appl. Sci.* **2021**, *11*, 2000. [[CrossRef](#)]
16. Shankar, A.N.; Chopade, S.; Srinivas, R.; Kumar Mishra, N.; Eftikhaar, H.K.; Sethi, G.; Singh, B. Physical and Mechanical Properties of Foamed Concrete, a Literature Review. *Mater. Today Proc.* **2023**, S2214785323050125. [[CrossRef](#)]
17. Othuman Mydin, M.A.; Wang, Y.C. Thermal and Mechanical Properties of Lightweight Foamed Concrete at Elevated Temperatures. *Mag. Concr. Res.* **2012**, *64*, 213–224. [[CrossRef](#)]
18. Fu, Y.; Wang, X.; Wang, L.; Li, Y. Foam Concrete: A State-of-the-Art and State-of-the-Practice Review. *Adv. Mater. Sci. Eng.* **2020**, *2020*, 6153602. [[CrossRef](#)]
19. Amran, Y.H.M.; Farzadnia, N.; Abang Ali, A.A. Properties and Applications of Foamed Concrete; A Review. *Constr. Build. Mater.* **2015**, *101*, 990–1005. [[CrossRef](#)]
20. Li, T.; Huang, F.; Zhu, J.; Tang, J.; Liu, J. Effect of Foaming Gas and Cement Type on the Thermal Conductivity of Foamed Concrete. *Constr. Build. Mater.* **2020**, *231*, 117197. [[CrossRef](#)]

21. Gökçe, H.S.; Hatungimana, D.; Ramyar, K. Effect of Fly Ash and Silica Fume on Hardened Properties of Foam Concrete. *Constr. Build. Mater.* **2019**, *194*, 1–11. [[CrossRef](#)]
22. Hosseinzadehfard, E.; Mobaraki, B. Investigating Concrete Durability: The Impact of Natural Pozzolan as a Partial Substitute for Microsilica in Concrete Mixtures. *Constr. Build. Mater.* **2024**, *419*, 135491. [[CrossRef](#)]
23. Raj, A.; Sathyan, D.; Balaji, K.; Mini, K.M. Heat Transfer Simulation across a Building Insulated with Foam Concrete Wall Cladding. *Mater. Today Proc.* **2021**, *42*, 1442–1446. [[CrossRef](#)]
24. Li, Z.; Su, S.; Jin, X.; Xia, M.; Chen, Q.; Yamashita, K. Stochastic and Distributed Optimal Energy Management of Active Distribution Network with Integrated Office Buildings. *CSEE J. Power Energy Syst.* **2022**, *10*, 1–14. [[CrossRef](#)]
25. Yang, X.; Lu, T.; Kim, T. Effective Thermal Conductivity Modelling for Closed-Cell Porous Media with Analytical Shape Factors. *Transp. Porous Media* **2013**, *100*, 211–224. [[CrossRef](#)]
26. Maxwell, J.C. A Treatise on Electricity and Magnetism. *Nature* **1873**, *7*, 478–480. [[CrossRef](#)]
27. Landauer, R. The Electrical Resistance of Binary Metallic Mixtures. *J. Appl. Phys.* **1952**, *23*, 779–784. [[CrossRef](#)]
28. Randrianalisoa, J.; Baillis, D. Thermal Conductive and Radiative Properties of Solid Foams: Traditional and Recent Advanced Modelling Approaches. *Comptes Rendus Phys.* **2014**, *15*, 683–695. [[CrossRef](#)]
29. Kirkpatrick, S. Percolation and Conduction. *Rev. Mod. Phys.* **1973**, *45*, 574–588. [[CrossRef](#)]
30. Sharma, N.K. Finite Element Modelling and Simulations on Effective Thermal Conductivity of Particulate Composites. *J. Therm. Anal. Calorim.* **2022**, *147*, 3441–3452. [[CrossRef](#)]
31. Chai, J.C.; Lee, H.S.; Patankar, S.V. Treatment of Irregular Geometries Using a Cartesian Coordinates Finite-Volume Radiation Heat Transfer Procedure. *Numer. Heat Transf. Part B Fundam.* **1994**, *26*, 225–235. [[CrossRef](#)]
32. Mendes, M.A.A.; Talukdar, P.; Ray, S.; Trimis, D. Detailed and Simplified Models for Evaluation of Effective Thermal Conductivity of Open-Cell Porous Foams at High Temperatures in Presence of Thermal Radiation. *Int. J. Heat Mass Transf.* **2014**, *68*, 612–624. [[CrossRef](#)]
33. Zeng, R.; Wang, K.; Li, P. Special Finite Elements with Arbitrarily-Shaped Holes for Heat Conduction Analysis of Porous Materials. *Int. J. Heat Mass Transf.* **2023**, *215*, 124458. [[CrossRef](#)]
34. Tian, X.; Birk, C.; Du, C.; Ooi, E.T. Automatic Micro-Scale Modelling and Evaluation of Effective Properties of Highly Porous Ceramic Matrix Materials Using the Scaled Boundary Finite Element Method. *Comput. Methods Appl. Mech. Eng.* **2024**, *419*, 116596. [[CrossRef](#)]
35. Langer, S.A.; Fuller, E.R.; Carter, W.C. OOF: An Image-Based Finite-Element Analysis of Material Microstructures. *Comput. Sci. Eng.* **2001**, *3*, 15–23. [[CrossRef](#)]
36. Luo, M.; Wang, C.; Zhao, J.; Liu, L. Characteristics of Effective Thermal Conductivity of Porous Materials Considering Thermal Radiation: A Pore-Level Analysis. *Int. J. Heat Mass Transf.* **2022**, *188*, 122597. [[CrossRef](#)]
37. Coquard, R.; Baillis, D. Numerical Investigation of Conductive Heat Transfer in High-Porosity Foams. *Acta Mater.* **2009**, *57*, 5466–5479. [[CrossRef](#)]
38. Miled, K.; Limam, O. Effective Thermal Conductivity of Foam Concretes: Homogenization Schemes vs Experimental Data and FEM Simulations. *Mech. Res. Commun.* **2016**, *76*, 96–100. [[CrossRef](#)]
39. Wei, S.; Yiqiang, C.; Yunsheng, Z.; Jones, M.R. Characterization and Simulation of Microstructure and Thermal Properties of Foamed Concrete. *Constr. Build. Mater.* **2013**, *47*, 1278–1291. [[CrossRef](#)]
40. Zhao, Z.; Qu, X.; Pang, J.; Yang, X.; Wen, H.; Yu, C.; Chen, C.; Tian, C.; Li, Z.; Zhao, S. Numerical Simulation of Pore Structure and Heat Transfer Behavior in Aerated Concrete. *Constr. Build. Mater.* **2023**, *364*, 129934. [[CrossRef](#)]
41. Progelhof, R.C.; Throne, J.L.; Ruetsch, R.R. Methods for Predicting the Thermal Conductivity of Composite Systems: A Review. *Polym. Eng. Sci.* **1976**, *16*, 615–625. [[CrossRef](#)]
42. Sepehri, E.; Siavashi, M. Pore-Scale Direct Numerical Simulation of Fluid Dynamics, Conduction and Convection Heat Transfer in Open-Cell Voronoi Porous Foams. *Int. Commun. Heat Mass Transf.* **2022**, *137*, 106274. [[CrossRef](#)]
43. Fan, C.; Xia, X.-L.; Du, W.; Sun, C.; Li, Y. Numerical Investigations of the Coupled Conductive-Radiative Heat Transfer in Alumina Ceramics. *Int. Commun. Heat Mass Transf.* **2022**, *135*, 106097. [[CrossRef](#)]
44. Li, Z.; Yang, M.; Zhang, Y. A Coupled Lattice Boltzmann and Finite Volume Method for Natural Convection Simulation. *Int. J. Heat Mass Transf.* **2014**, *70*, 864–874. [[CrossRef](#)]
45. Wei, Y.; Liu, X.; Zhu, K.; Huang, Y. A Unified Lattice Boltzmann Framework for Combined Radiation-Conduction Heat Transfer. *Int. J. Heat Mass Transf.* **2023**, *200*, 123513. [[CrossRef](#)]
46. Skochdopole, R.E. The Thermal Conductivity of Foamed Plastics. *Chem. Eng. Prog.* **1961**, *57*, 55–59.
47. Collishaw, P.G.; Evans, J.R.G. An Assessment of Expressions for the Apparent Thermal Conductivity of Cellular Materials. *J. Mater. Sci.* **1994**, *29*, 2261–2273. [[CrossRef](#)]
48. Vesenjajk, M.; Žunič, Z.; Öchsner, A.; Hriberšek, M.; Ren, Z. Heat conduction in closed-cell cellular metals. *Mater. Werkst.* **2005**, *36*, 608–612. [[CrossRef](#)]
49. Ma, X.; Li, H.; Wang, D.; Li, C.; Wei, Y. Simulation and Experimental Substantiation of the Thermal Properties of Non-Autoclaved Aerated Concrete with Recycled Concrete Powder. *Materials* **2022**, *15*, 8341. [[CrossRef](#)]

50. Rivera-Salinas, J.-E.; Gregorio-Jáuregui, K.-M.; Fonseca-Florido, H.-A.; Ávila-Orta, C.-A.; Ramírez-Vargas, E.; Romero-Serrano, J.-A.; Cruz-Ramírez, A.; Gutiérrez-Pérez, V.-H.; Olvera-Vazquez, S.-L.; Rosales-Marines, L. Numerical Study Using Microstructure Based Finite Element Modeling of the Onset of Convective Heat Transfer in Closed-Cell Polymeric Foam. *Polymers* **2021**, *13*, 1769. [[CrossRef](#)]
51. Bergman, T.L.; Lavine, A.S.; Incropera, F.P.; DeWitt, D.P. *Fundamentals of Heat and Mass Transfer*, 8th ed.; Global Edition; Wiley: Hoboken, NJ, USA, 2017; ISBN 978-1-119-38291-1.
52. Johnson, N.L.; Kemp, A.W.; Kotz, S. *Univariate Discrete Distributions*, 1st ed.; Wiley Series in Probability and Statistics; Wiley: Hoboken, NJ, USA, 2005; ISBN 978-0-471-27246-5.

**Disclaimer/Publisher's Note:** The statements, opinions and data contained in all publications are solely those of the individual author(s) and contributor(s) and not of MDPI and/or the editor(s). MDPI and/or the editor(s) disclaim responsibility for any injury to people or property resulting from any ideas, methods, instructions or products referred to in the content.